SYSTEMS BIOLOGY

Integrative analysis of kinase networks in TRAIL-induced apoptosis provides a source of potential targets for combination therapy

Jonathan So,[1,2] Adrian Pasculescu,[1] Anna Y. Dai,[1] Kelly Williton,[1] Andrew James,[1]* Vivian Nguyen,[1] Pau Creixell,[3] Erwin M. Schoof,[3] John Sinclair,[4] Miriam Barrios-Rodiles,[1] Jun Gu,[1†] Aldis Krizus,[1‡] Ryan Williams,[1] Marina Olhovsky,[1] James W. Dennis,[1,5] Jeffrey L. Wrana,[1,5] Rune Linding,[3,6§] Claus Jorgensen,[4§¶] Tony Pawson,[1,2,5‖] Karen Colwill[1§]

Tumor necrosis factor–related apoptosis–inducing ligand (TRAIL) is an endogenous secreted peptide and, in preclinical studies, preferentially induces apoptosis in tumor cells rather than in normal cells. The acquisition of resistance in cells exposed to TRAIL or its mimics limits their clinical efficacy. Because kinases are intimately involved in the regulation of apoptosis, we systematically characterized kinases involved in TRAIL signaling. Using RNA interference (RNAi) loss-of-function and cDNA overexpression screens, we identified 169 protein kinases that influenced the dynamics of TRAIL-induced apoptosis in the colon adenocarcinoma cell line DLD-1. We classified the kinases as sensitizers or resistors or modulators, depending on the effect that knockdown and overexpression had on TRAIL-induced apoptosis. Two of these kinases that were classified as resistors were PX domain–containing serine/threonine kinase (PXK) and AP2-associated kinase 1 (AAK1), which promote receptor endocytosis and may enable cells to resist TRAIL-induced apoptosis by enhancing endocytosis of the TRAIL receptors. We assembled protein interaction maps using mass spectrometry–based protein interaction analysis and quantitative phosphoproteomics. With these protein interaction maps, we modeled information flow through the networks and identified apoptosis-modifying kinases that are highly connected to regulated substrates downstream of TRAIL. The results of this analysis provide a resource of potential targets for the development of TRAIL combination therapies to selectively kill cancer cells.

INTRODUCTION

A key challenge in cancer therapy is to specifically target tumor cells while sparing normal cells. Hence, the discovery that the protein tumor necrosis factor–related apoptosis–inducing ligand (TRAIL) preferentially induces apoptosis of cancerous cells (*1*) led to concentrated efforts to better understand this pathway and to develop therapeutics to mimic this selectively toxic effect of TRAIL (*2*). TRAIL initiates apoptosis by binding to the TRAIL receptors TRAIL-R1 or TRAIL-R2, which are also known as tumor necrosis factor receptor superfamily members 10a or 10b (TNFRSF10A, TNFRSF10B), and triggering the recruitment of caspase 8 (CASP8) and Fas-associated protein with death domain (FADD) to the receptors to form the death-inducing signaling complex (*3*). CASP8 is then activated by autocatalytic cleavage and cleaves CASP3, which activates CASP3. Active CASP3 promotes apoptosis by cleaving downstream substrates (*4*). In addition, an intrinsic pathway further amplifies the apoptotic signal; CASP8 cleaves the B cell CLL/lymphoma 2 (BCL-2) family member BH3-interacting domain death agonist (BID), leading to its mitochondrial relocation where, together with other proapoptotic BCL-2 proteins, BID promotes the release of cytochrome c. Once in the cytoplasm, cytochrome c forms the "apoptosome" complex with apoptosis protease factor 1 (APAF1) and CASP9, which also activates CASP3 to augment the apoptotic process.

Reports from clinical trials indicate that many tumors are either intrinsically resistant or rapidly acquire resistance to TRAIL, thereby limiting its effectiveness (*5*–*7*). Protein kinases regulate apoptosis and are linked to the emergence of TRAIL resistance. For instance, activation of the epidermal growth factor receptor (EGFR), a receptor tyrosine kinase, inhibits TRAIL-induced apoptosis, mainly through activation of the kinase AKT (*8*). Consistent with this observation, inhibition of the phosphatidylinositol 3′-kinase (PI3K)–AKT pathway restores TRAIL sensitivity (*9*–*11*). Inactivation of caspases is another common mechanism through which kinases promote resistance (*12*). Signaling by the TRAIL receptor activates multiple kinases, such as inhibitor of nuclear factor κB (IκB) kinases (IKKs), c-Jun N-terminal kinases (JNKs), and p38 mitogen-activated protein kinase (p38), which can increase the expression of pro- or antiapoptotic genes, such as those encoding X-linked inhibitor of apoptosis (XIAP) and FADD-like apoptosis regulator (CFLAR), which are antiapoptotic, and CASP8, which is proapoptotic (*10*, *13*–*15*). In colorectal cancer cell lines, TRAIL stimulation

[1]Lunenfeld-Tanenbaum Research Institute, Mount Sinai Hospital, Toronto, Ontario M5G 1X5, Canada. [2]Institute of Medical Science, University of Toronto, Toronto, Ontario M5S 1A8, Canada. [3]Cellular Signal Integration Group (C-SIG), Technical University of Denmark (DTU), DK-2800 Lyngby, Denmark. [4]Cell Communication Team, The Institute of Cancer Research, London SW3 6JB, UK. [5]Department of Molecular Genetics, University of Toronto, Toronto, Ontario M5S 1A8, Canada. [6]Biotech Research and Innovation Centre (BRIC), University of Copenhagen (UCPH), DK-2200 Copenhagen, Denmark.
*Present address: Sanofi-Pasteur, Toronto, Ontario M2R 3T4, Canada.
†Present address: Terrence Donnelly Centre for Cellular and Biomolecular Research (CCBR), University of Toronto, 160 College Street, Toronto, Ontario M5S 3E1, Canada.
‡Present address: Department of Molecular Genetics, University of Toronto, Toronto, Ontario M5S 1A8, Canada.
§Corresponding authors. E-mail: linding@lindinglab.org (R.L.); claus.jorgensen@cruk.manchester.ac.uk (C.J.); colwill@lunenfeld.ca (K.C.)
¶Present address: Systems Oncology Group, Cancer Research UK Manchester Institute, The University of Manchester, Wilmslow Road, Manchester M20 4BX, UK.
‖Deceased.

promotes the release of transforming growth factor–α (TGFα), a ligand that stimulates the EGFR and ERBB2 (v-erb-b2 avian erythroblastic leukemia viral oncogene homolog 2) prosurvival pathways (*16*).

Crosstalk among pathways can impart cellular signaling networks with a robustness that is essential for accurate response to cellular cues, because robust networks are tolerant of physiological noise. However, crosstalk also provides mechanisms for tumor cells to rewire their signaling to circumvent drug-induced inhibition. The more tolerant a network is to perturbations, the more fragile it may be to multiple, well-targeted hits, a condition dubbed "highly optimized tolerance (HOT) fragility" (*17, 18*). Thus, network fragility can be leveraged therapeutically by inhibiting a specific combination of targets, a concept pertinent to the emerging field of network medicine (*19, 20*). Therefore, identifying kinase inhibitors that cooperate with TRAIL or TRAIL-like agonists to block tumor growth or the development of resistance could be beneficial for cancer treatment. Computational approaches can help predict the most effective combination of targets, and evidence suggests that these approaches do not require that all network connections and signaling dynamics are fully known or included. For example, models based on graph theory related network connectivity with phenotypes, such as for cancer survival and gene essentiality (*21–24*), and biological models based on electrical circuitry have been used to identify proteins that were associated with loss-of-function–induced cell lethality (*25*).

Here, we systematically screened for protein kinases that have a functional impact on TRAIL-induced apoptosis using knockdown and overexpression in DLD-1 colorectal carcinoma cells. To map underlying signaling network that controlled the phenotypic responses, we affinity-captured selected kinases and analyzed protein interaction partners by mass spectrometry (MS) and constructed a network that we integrated with kinase-substrate pairs predicted from a global phosphoproteomics analysis. By relating connectivity with phenotype through network modeling of information flow, we identified kinases involved in TRAIL signaling and present these as a resource of potential drug targets in conjunction with TRAIL.

RESULTS

A small interfering RNA screen identifies kinases involved in TRAIL-induced caspase activation

Protein kinases influence virtually every aspect of cellular regulation, including programmed cell death (*26–28*). Thus, we reasoned that perturbation of the abundance of individual kinases would identify kinases that modulate the ability of TRAIL to promote apoptosis in cancer cells. To identify kinases that affect TRAIL-induced apoptosis, we performed both small interfering RNA (siRNA) knockdown and overexpression experiments of kinases in the TRAIL-responsive colorectal cancer cell line DLD-1.

For siRNA knockdown studies, we transfected DLD-1 cells with the human kinome siRNA library (siGenome, GE Healthcare Dharmacon) that targets 715 transcripts, of which 496 encode protein kinases and the remainder encode other kinase types, such as kinases involved in metabolism or lipid kinases, or kinase regulatory proteins, for example, cyclin-dependent kinase (CDK) inhibitor 1A (CDKN1A). We monitored the dynamics of apoptosis induction using a fluorescence resonance energy transfer (FRET) reporter (EC-RP) containing a CASP3 consensus cleavage sequence (DEVDR) sandwiched between enhanced cyan fluorescent protein (CFP) and the Venus fluorophore (*29*). We used fluorescence polarization (FP) to monitor FRET, which provided a sensitive, real-time assay to measure apoptosis in a high-throughput screen [a strategy adapted from (*30*); see fig. S1]. Unlike intensity-based FRET measurements, FP requires no normalization for the amount of sensor transfected and is less susceptible to measurement noise (*31*). We measured the FP of EC-RP to monitor CASP3 activity as a surrogate for apoptosis over a 5-hour time course (fig. S2).

We used hierarchical clustering to classify the results of the siRNA screen into kinases that sensitized the cells to TRAIL-induced apoptosis, kinases that enabled resistance to TRAIL-induced apoptosis, and kinases that did not affect the TRAIL-induced response (Fig. 1A). We removed seven siRNA targets from the data set because of low fluorescent signal or large variability between time points (fig. S2, "outliers" in table S1). We normalized the FP values of the remaining 708 targets, including the control siRNA targeting glyceraldehyde-3-phosphate dehydrogenase (GAPDH), to the initial $t = 0$ time point to account for differences in background cleavage of the reporter. We defined "sensitizers" as those targets that, when depleted, decreased the proportion of cells undergoing apoptosis (the cells with these siRNAs displayed slower kinetics of TRAIL-induced EC-RP activation) relative to the control and to siRNA against other targets; these sensitizers promote apoptosis. Similarly, a target that when knocked down increased apoptosis is defined as a "resistor." siRNA targets that did not affect TRAIL-induced EC-RP activation to the same extent as the sensitizers or resistors were viewed as "neutral." The effect of knockdown on the dynamics of the TRAIL-induced apoptotic response, detected as EC-RP cleavage, showed that controls (neutral control, GAPDH; resistor control, CFLAR; sensitizer control, CASP8) were classified into the appropriate groups (Fig. 1B). Additionally, IκB kinase β (IKBKB), which activates the transcription factor NF-κB and thereby prevents apoptosis in some contexts (*32*), and receptor-interacting serine-threonine kinase 2 (RIPK2), which contains a C-terminal caspase activation and recruitment domain (CARD) domain that recruits caspases (*33, 34*), were properly classified into the resistor and sensitizer groups, respectively (Fig. 1B).

On the basis of hierarchical clustering, we classified 14% of the kinases as resistors (15% when limited to protein kinases) and 11% as sensitizers on the basis of their distinct patterns of response (Fig. 1C, fig. S2, and table S1). Furthermore, this hit rate is consistent with 34% of protein kinases having "apoptosis" or "apoptotic" in a Gene Ontology (GO) term name description (Fig. 1C and table S1).

To increase our confidence in this initial screen, we tested a panel of siRNAs (Qiagen) with alternative sequence and chemistry that were directed against the resistor control CFLAR, the sensitizer control CASP8, and a scrambled sequence to serve as a neutral control, along with five other targets [resistor in siRNA screen, Rho-associated coiled-coil–containing protein kinase 2 (ROCK2), CDK11A; neutral in siRNA screen, interleukin-1 receptor–associated kinase 1 (IRAK1); and sensitizer in siRNA screen, PAK1 and mitogen-activated protein kinase 3 (MAPK3)]. All except the siRNA targeting MAPK3 produced similar results for the effect of knockdown of the target on CASP3 activity using the EC-RP sensor as were observed in the siRNA screen (fig. S3A). As an alternative measure of apoptosis, we also confirmed that individual knockdown of a subset of the resistor kinases increased DNA fragmentation after 4 hours of TRAIL treatment (fig. S3B). In the initial siRNA screen, we did not observe any effect of individually targeting the TRAIL receptors, TNFRSF10A and TNFRSF10B. To test whether the receptors acted in a redundant manner, we retested the effect of targeting these individually or in combination using propidium iodide (PI) staining. TNFRSF10A knockdown was neutral in this assay of apoptosis, TNFRS10B knockdown appeared to increase apoptosis, and the depletion of both receptors reduced apoptosis (fig. S3), consistent with functional redundancy of the receptors (*35*).

An overexpression screen identifies kinases involved in TRAIL-induced caspase activation

To complement the siRNA screen data and to control for false-positive and false-negative identifications, we performed a gain-of-function screen

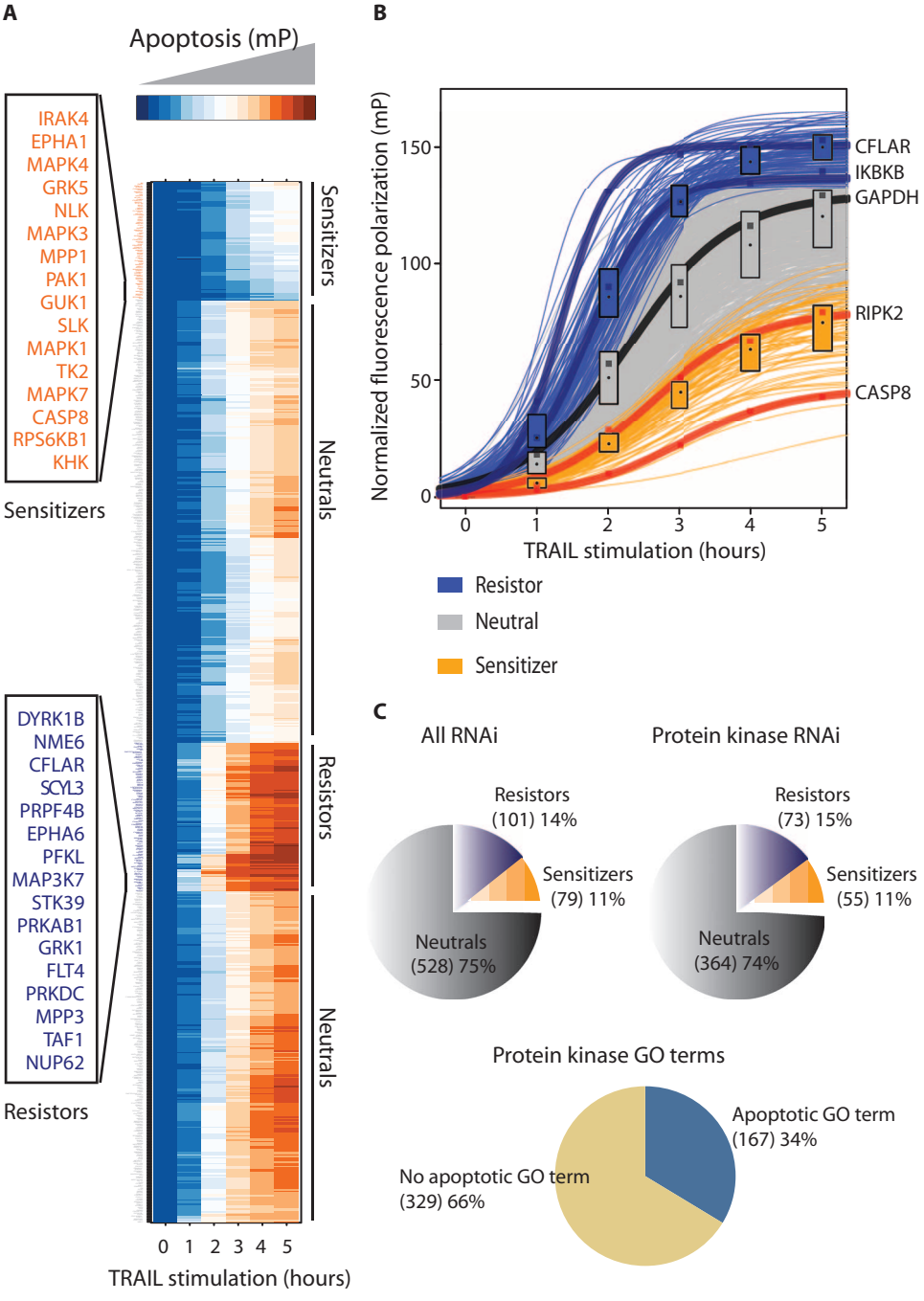

Fig. 1. RNAi screen to identify kinases that modulate TRAIL-induced apoptosis. (**A**) Hierarchical clustering (distance: Euclidean, method: complete) of the median increase in fluorescence polarization (FP) of the CASP3 sensor over a 5-hour time course (normalized to t = 0 hour) after TRAIL stimulation and gene knockdown by siRNA. Kinases in the neutral, sensitizer, and resistor groups were significantly different from one another by Hotelling's T^2 test ($P < 10^{-16}$, $n = 2$). Representative kinases classified as sensitizers and resistors in the region including the controls sensitizer control CASP8 and resistor control CFLAR are shown. mP, millipolarization. (**B**) The median FP response of all siRNA at each time point (normalized to t = 0 hour), showing the separation of neutrals, resistors, and sensitizers. The boxes represent 1 SD above and below the median. Selected siRNA targets are labeled. (**C**) Summary of the screen results for all RNAi targets and a subset containing only protein kinases, as well as the percentage of protein kinases that have a GO term name containing "apoptosis" or "apoptotic."

for ectopically expressed kinases that affected TRAIL sensitivity. We selected kinases for overexpression on the basis of the availability of full-length complementary DNA (cDNA) and because these kinases represent different kinase families. We created 107 stable DLD-1 cell lines expressing individual nonreceptor protein kinases fused at the N terminus to a triple-FLAG tag (table S2). To estimate the effects of kinase overexpression on apoptosis, we stimulated the cell lines with TRAIL for 2 or 4 hours, labeled cells with antibodies for cleaved CASP3 and cleaved poly(ADP-ribose) polymerase (PARP), and performed flow cytometry (fig. S4A).

Overexpression of casein kinase 2 α-1 (CSNK2A1), an antiapoptotic protein (*36*), promoted resistance to TRAIL, whereas overexpression of the oncogenic serine/threonine kinase ARAF (also known as A-Raf) increased TRAIL-induced cleavage of CASP3 and PARP (Fig. 2A). Applying the same nomenclature used to classify the targets identified in the siRNA screen, we refer to CSNK2A1 as a resistor and ARAF as a sensitizer. We then used these two as positive controls to identify other resistor or sensitizer kinases. We used Hotelling's T^2 test to determine if the effect of TRAIL on cells expressing the other kinases was significantly different from those expressing CSNK2A1 or ARAF or transfected with a negative control vector (neutral) (fig. S4B). If a kinase was not significantly different from any of these controls (neutral, resistor, or sensitizer), we considered the kinase as "unclassified" (fig. S4C and table S3). By this method, 21 kinases were termed "unclassified." Overexpression of 50% of kinases caused a resistor (47 kinases) or sensitizer (6 kinases) phenotype (Fig. 2, B and C). Overexpression of 33 kinases had a similar effect to the negative control and were classified as neutrals. Interleukin-1 receptor–associated kinase 4 (IRAK4), which produced the most resistance when overexpressed, was manually assigned a phenotype because the Hotelling values comparing it to the controls were 0.

We compared the 104 kinases tested in both the cDNA and siRNA screens [microtubule associated serine/threonine kinase 1 (MAST1) and SCY1-like 2 (SCYL2) were not tested, and protein tyrosine kinase 2 (PTK2) was an outlier in the siRNA screen] (table S4 and Fig. 2D), because we predicted that kinases positive in both screens would be higher-confidence candidates for a role in TRAIL-mediated apoptosis. Because there was insufficient evidence to state that unclassified kinases in the cDNA screen

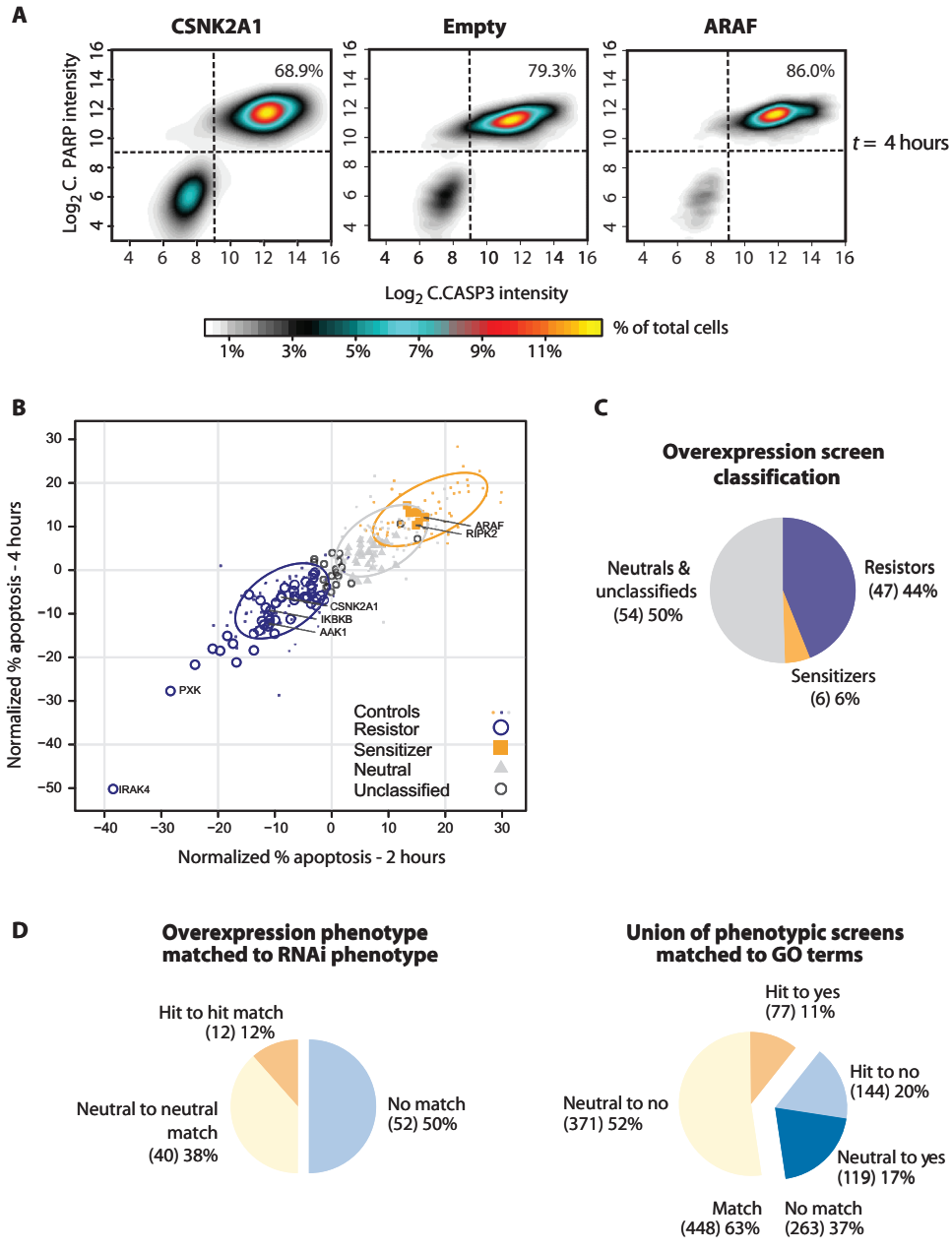

Fig. 2. Overexpression screen to identify protein kinases that modulate TRAIL-induced apoptosis. (**A**) Representative dot plots of cells sorted by flourescence-activated cell sorting (FACS) on the basis of cleaved PARP intensity and cleaved CAPS3 intensity 4 hours after TRAIL stimulation for the three controls. The percentage of apoptotic cells (cleaved PARP$^+$ and cleaved CASP3$^+$)/total number of cells is indicated in each plot. (**B**) Plot of the percent of apoptotic cells [determined as described in (A)] for each stable kinase-expressing cell line at 2 and 4 hours after TRAIL stimulation. The median values of each stable kinase cell line across replicates (minimum $n = 3$), normalized to $t = 0$ hour, and to the controls (CSNK2A1 and empty vector cell lines) are plotted. Hotelling's T^2 test was used to separate neutrals (gray triangles), sensitizers (orange squares), and resistors (blue circles). All data points for the controls (ARAF—sensitizer; empty vector—neutral; CSNK2A1—resistor) are shown as small dots. An open oval encloses the 70% quantile of the data points for each. Kinases that could not be classified by comparison with the controls appear as open black circles. IRAK4 was manually assigned a phenotype. Selected kinases are identified. (**C**) Summary of the overexpression screen results. (**D**) Comparison of the results between the two screens with a hit defined as a kinase with an apoptosis-modifying phenotype. The combined phenotypes from the union of these two screens (table S4) were compared to GO terms. If a GO term name for a protein contained "apoptosis" or "apoptotic," the protein was considered an influencer of apoptosis (labeled "yes"); otherwise, the protein was labeled with "no" apoptotic GO term. The number of proteins in each category and the percentage are indicated.

influenced apoptosis, we considered them the same as neutral. Of the 104 kinases, 50% had consistent results between screens: 40 were neutral and 12 altered caspase activity (Fig. 2D and Table 1). Eight of the 12 kinases—G protein (heterotrimeric guanine nucleotide–binding protein)–coupled receptor kinase 1 (GRK1), IKBKB, integrin-linked kinase (ILK), IRAK4, maternal embryonic leucine zipper kinase (MELK), RIPK2, ROCK2, and tyrosine kinase nonreceptor 1 (TNK1)—that altered caspase activity have known roles in apoptosis, and four were novel—AP2 associated kinase 1 (AAK1), PX domain containing serine/threonine kinase (PXK), serine/threonine/tyrosine kinase 1 (STYK1), and testis-specific serine kinase 1B (TSSK1B). The results from the knockdown or overexpression analysis produced concordant functional effects for AAK1, GRK1, IKBKB, PXK, RIPK2, ROCK2, STYK1, and TSSK1B, whereas ILK, IRAK4, MELK, and TNK1 had phenotypes that were discordant between screens (termed "modulators"), suggesting that they may have either pro- or antiapoptotic roles in cells exposed to TRAIL, depending on the relative abundance of the kinase (Table 1).

From the union of the two screens, we identified 221 proteins (169 protein kinases) as hits: 137 resistors (109 protein kinases), 80 sensitizers (56 protein kinases), and 4 modulators (all of which were protein kinases) (table S4), which we refer to herein as apoptosis-modifying. From the union, 63% correlate with having an "apoptotic" GO term assigned to them (for hits) or no "apoptotic" GO term (for neutrals) (Fig. 2D). The hits mapped broadly among kinase families (fig. S5), consistent with apoptosis being a phenomenon that involves diverse signaling pathways.

We tested TRAIL-induced cell death in two additional colon cancer cell lines in which we depleted various kinases identified as resistors in

Table 1. Kinases that show a phenotype in both the siRNA and overexpression screens.

Kinase	siRNA phenotype	Overexpression phenotype	Combined phenotype	Previous link to apoptosis*
AAK1	Resistor	Resistor	Resistor	Novel
GRK1	Resistor	Resistor	Resistor	(*114*) (*115*) (*116*)
IKBKB	Resistor	Resistor	Resistor	(*32*) (*117*) (*118*)
ILK	Sensitizer	Resistor	Modulator	(*119*) (*120*) (*121*)
IRAK4	Sensitizer	Resistor	Modulator	(*122*) (*123*) (*124*)
MELK	Sensitizer	Resistor	Modulator	(*125*)
PXK	Resistor	Resistor	Resistor	Novel
RIPK2	Sensitizer	Sensitizer	Sensitizer	(*126*) (*34*) (*33*)
ROCK2	Resistor	Resistor	Resistor	(*127*) (*128*) (*129*)
STYK1	Resistor	Resistor	Resistor	Novel
TNK1	Sensitizer	Resistor	Modulator	(*130*) (*131*)
TSSK1B	Resistor	Resistor	Resistor	Novel

*A maximum of 3 literature reports are listed.

the DLD-1 cells (fig. S6). Like the DLD-1 cells, which have an activating mutation in K-Ras (G13D), the two cell lines each have distinct activating mutations in RAS: HCT116 has K-Ras^{G13D} and LS174 has K-Ras^{G12D}. The analysis showed that HCT116 cells responded similarly to the DLD-1 cells in terms of the increase in TRAIL sensitivity when AAK1, PXK, IKBKB, ROCK2, or CDK11A was depleted. However, the positive control resistor CFLAR in the DLD-1 cells was not important for TRAIL resistance in HCT116 cells. In contrast, LS174 cells were strongly affected by depletion of CFLAR, but only showed increased sensitivity to TRAIL-induced apoptosis when depleted of AAK1, ROCK2, or CDK11A (fig. S6). Thus, these data suggest that the influence of these kinases on TRAIL-mediated apoptosis extends beyond DLD-1 cells, but that there are some cell-specific differences.

Immunoprecipitation-MS defines a protein-protein interaction network for kinases in DLD-1 cells

To probe the molecular basis for the observed phenotypes in our screens, we created an interaction network by systematically immunoprecipitating FLAG-tagged kinases from the stably transfected DLD-1 cells and identifying interacting partners ("preys") by MS (IP-MS) (table S5). Of the 108 kinases analyzed [table S2, 107 from the overexpression screen plus adrenergic beta receptor kinase 1 (ADRBK1)], we excluded 4 from the final analysis because of their low abundance in the MS results (<10% coverage of the bait kinase). We removed nonspecific interactions and "bait carryover" from the MS results (fig. S7). We confirmed a subset of the remaining interactions by coimmunoprecipitation (Table 2 and fig. S8), including several known interactions [CDK2 with MAPK15 (*37*), CDK5 with cyclin I (CCNI) (*37*), and RIO kinase 1 (RIOK1) with protein arginine methyltransferase 5 (PRMT5) (*38*)], as well as previously

Table 2. Interacting partners validated by immunoprecipitation.

Kinase	Partner	Positive in reciprocal coIPs	Previously reported
JAK3	NAP1L1	Yes	No
JAK3	MAGED2	Yes	No
CDK2	MAPK15	Yes	Yes (*37*)
CDK5	CCNI	Yes	Yes (*37*)
STK11	COPS4	Yes	No
CASK	SNTB2	Yes	No
PRKCB	SHCBP1	Only in 1 IP	No
TRIB1	STK40	Only in 1 IP	No
IKBKE	APPBP2	Yes	No
PRMT5	RIOK1	Yes	Yes (*38*)

uncharacterized interactions [Janus kinase 3 (JAK3) with nucleosome assembly protein 1–like 1 (NAP1L1) and melanoma antigen family D2 (MAGED2), serine/threonine kinase 11 (STK11) with COP9 signalosome subunit 4 (COPS4), protein kinase Cβ (PRKCB) with SHC SH2 (Src homology 2) domain binding protein 1 (SHCBP1), IκB kinase ε (IKBKE) with amyloid β precursor protein binding protein 2 (APPBP2), tribbles pseudokinase 1 (TRIB1) with serine/threonine kinase 40 (STK40), and calcium/calmodulin-dependent serine protein kinase (CASK) with syntrophin β2 (SNTB2)].

Because the position of the tag may influence the interaction of the bait with prey proteins, we selected a subset of kinases for expression in a C-terminal triple-FLAG vector with a stronger promoter [cytomegalovirus (CMV) instead of long terminal repeat (LTR)] and subjected them to IP-MS. The test set included 11 kinases: 3 where the N-terminal tag blocked a known myristoylation signal (SRC, BLK, ABL1), 3 that had few preys [microtubule-associated serine/threonine kinase 3 (MAST3), AKT1, STK11], 4 that we identified as apoptosis-modifying [ARAF, death-associated protein kinase 1 (DAPK1), IKBKB, protein kinase Cζ (PRKCZ)], and 1 positive control (CDK2). Preys were identified and processed in a similar manner to the previous analysis (fig. S6). Using this method, we identified 264 additional interactions and recapitulated 56 interactions that were seen with the N-terminal FLAG-tagged constructs (table S5), supporting the notion that the position of the tag influences which partners are identified (*22*). In particular, we identified additional interactions for kinases in which the N-terminal tag interfered with protein myristoylation: ABL1 interacted with multiple members of the 14-3-3 family (YWHAB, YWHAE, YWHAG, YWHAH, YWHAQ, YWHAZ), only one of which (YWHAZ) was identified with the N terminus–tagged kinase, SRC bound 18 additional proteins including known interactors PTK2 (*39*) and breast cancer anti-estrogen resistance 1 (BCAR1) (*40*), and BLK bound 46 additional proteins including members of the mitochondrial adenosine triphosphate (ATP) synthase complex. Switching the tag to the C terminus only led to the identification of one additional protein partner for AKT1. However, STK11 tagged at the C terminus bound additional members of the signalosome complex (COPS2, COPS3, and COPS6 in addition to COPS4 that was identified with the N terminus–tagged version). The signalosome complex is a multisubunit protease that inhibits the activity of the cullin–RING ligase (CRL) families of ubiquitin E3 complexes (*41*). For MAST3, 51 additional interacting proteins were identified, including interactions with kinases CSNK2A1, CSNK2A2, and protein kinase, AMP-activated α1 (PRKAA1). Combined with the N terminus data, the IP-MS network is composed of 1646 interacting pairs.

To assess the quality of our IP-MS network, we compared it to networks from two studies that identified protein kinase interactions through

IP-MS (*37, 42*). Our study had 10 kinase baits in common with Varjosalo *et al.* (*37*) and 8 kinase baits in common with Varjosalo *et al.* (*42*). There was an overlap of identified preys of 22 and 25%, respectively (fig. S9 and table S6), which is the typical reproducibility between IP-MS experiments (*42*). The lack of more preys in common likely reflects contextual differences between the cell lines, alternative expression and purification protocols, and methodological differences in data filtering.

Graphing the number of interacting partners for each kinase, separated into neutral and unclassified (neutral/unclassified) and those that were sensitizers or resistors (apoptosis-modifying), revealed that most kinases interacted with between 2 and 10 partners with the median number of interactions being 9 (8 for neutral/unclassified kinases, 10.5 for apoptosis-modifying kinases). There are more apoptosis-modifying kinases than neutral/unclassified kinases with more than 20 interacting partners, but this difference does not translate to a significantly higher degree (number of interactors) for apoptosis-modifying kinases (Fig. 3A, inset). Four of the top five most highly connected kinases [ARAF, IRAK1, LIM domain kinase 2 (LIMK2)], and a pseudokinase (ILK) that affected DLD-1 cells' sensitivity to TRAIL also shared protein interaction partners, including apoptosis-inducing factor, mitochondrion-associated 1 (AIFM1) and members of the catenin family (α- and β-catenin, CTNNA1, CTNNB1) (Fig. 3B), which may provide insight into the mechanisms by which these kinases influence TRAIL-mediated apoptosis.

AAK1 and PXK promote TRAIL receptor endocytosis

AAK1 and PXK modulated TRAIL sensitivity in both the siRNA and overexpression screens and had no previous links to apoptosis (Table 1). PXK, a sorting nexin, promotes the internalization and degradation of EGFR (*43*), and AAK1 promotes clathrin assembly through phosphorylation of the adaptor-related protein complex 2 μ1 (AP2M1) component of the AP2 complex (*44, 45*). As expected, members of the endocytotic pathway coimmunoprecipitated with both kinases—AAK1 with AP2 family proteins and PXK with clathrin subunits (Fig. 4A). Therefore, we hypothesized that the abundance of PXK and AAK1 may affect the endocytosis of TRAIL receptors. We assayed the uptake of FLAG-tagged TRAIL in serum-starved DLD-1 cells stably expressing either of the kinases (Fig. 4, B and C). After 60 min, cells overexpressing PXK or AAK1 internalized more FLAG-tagged TRAIL than did cells overexpressing IKBKB (a resistor that did not coimmunoprecipitate with endocytosis-related proteins and has no known role in endocytosis) or empty vector control (Fig. 4C). Thus, our results provide evidence that AAK1 and PXK promote TRAIL receptor endocytosis, which may explain the ability of AAK1 and PXK to function as resistors of TRAIL-mediated apoptosis.

Phosphoproteomic analysis identifies TRAIL-regulated phosphorylated proteins

Important regulatory associations may not have been captured in the IP-MS experiments because of the transient nature of many kinase-substrate interactions. Because we detected phosphorylated sites on the kinases and their binding partners (179 with high confidence by MS, as defined in Materials and Methods), we inferred the activity of transiently interacting regulatory kinases. We identified kinases known to phosphorylate these sites with PhosphoSitePlus (*46*), or we predicted kinases with the NetPhorest and NetworKIN algorithms (*47, 48*). This analysis expanded the IP-MS network from 1646 to1779 pairs by adding protein kinases for 120 phosphorylated sites and 15 predicted SH2 domain–containing partners for 9 phosphotyrosine motifs (table S5).

To identify additional kinase-substrate relationships affected by TRAIL stimulation, we performed phosphoproteomic analysis of TRAIL-stimulated DLD-1 cells. Stable isotope labeling by amino acids in cell culture (SILAC)

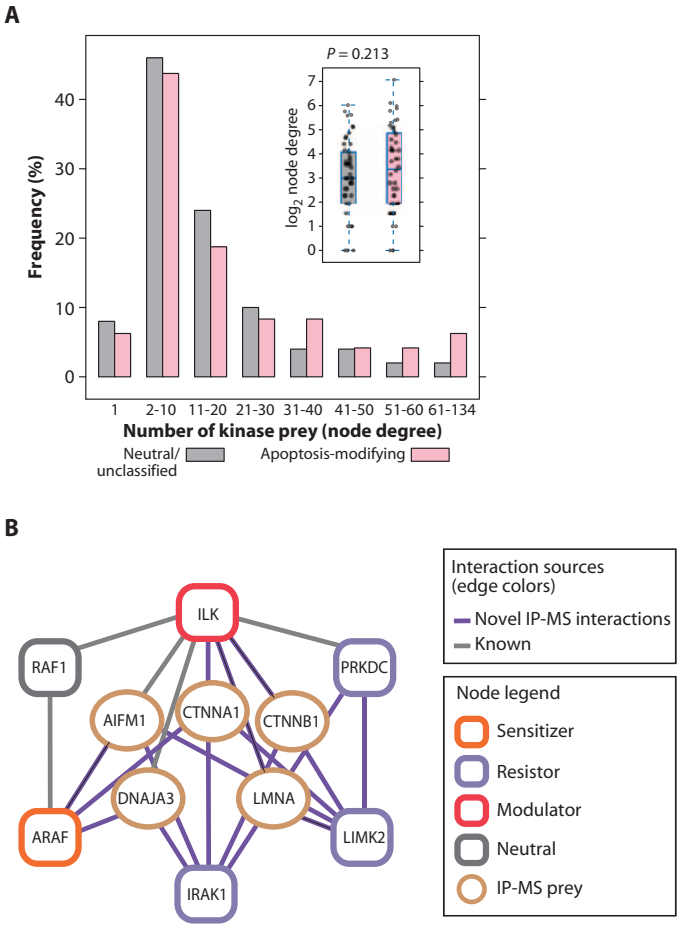

Fig. 3. Properties of the IP-MS network within DLD-1 cells. (A) Graph of the degree distribution of neutral or unclassified and apoptosis-modifying (sensitizer or resistor) kinases. The phenotypes correspond to those of the overexpression assay, which used the same stable cell lines as were used for the IP-MS assay. Inset is a box plot view of the node degree distribution for apoptosis-modifying kinases compared to neutral or unclassified kinases showing no significant enrichment for apoptosis-modifying kinases (P = 0.213, Wilcoxon one-tailed test). (B) A subnetwork of highly connected apoptosis-modifying kinases, with shared apoptosis-associated interacting proteins (IP-MS preys). RAF1 binding to ARAF was previously reported in (*113*), and the known interactions for ILK were reported in (*42*).

(*49*)–labeled DLD-1 cells were stimulated with TRAIL for 0, 5, or 60 min to capture both early and later downstream phosphorylation events, and peptides were analyzed by MS. From this analysis, we identified 4701 (2671 unique) phosphopeptides (table S7). We considered phosphopeptides with ratios between time points of TRAIL stimulation (for example, t5/t0, t60/t5, t60/t0) greater than 3 SDs compared to unphosphorylated peptides as significantly modulated, yielding 353 phosphopeptides (table S7 and figs. S10 and S11). Analysis of a subset of phosphorylation events by immunoblotting using phosphorylation site-specific antibodies indicated that selecting a threshold of 3 SDs was reasonable (fig. S12).

Phosphorylated sites that are modulated by TRAIL may play a role in propagating downstream signals. We used the PhosphoSitePlus database (*50*) and the NetworKIN algorithm (*51*) to predict kinases mediating phosphorylation at the sites represented by these phosphopeptides (table S7).

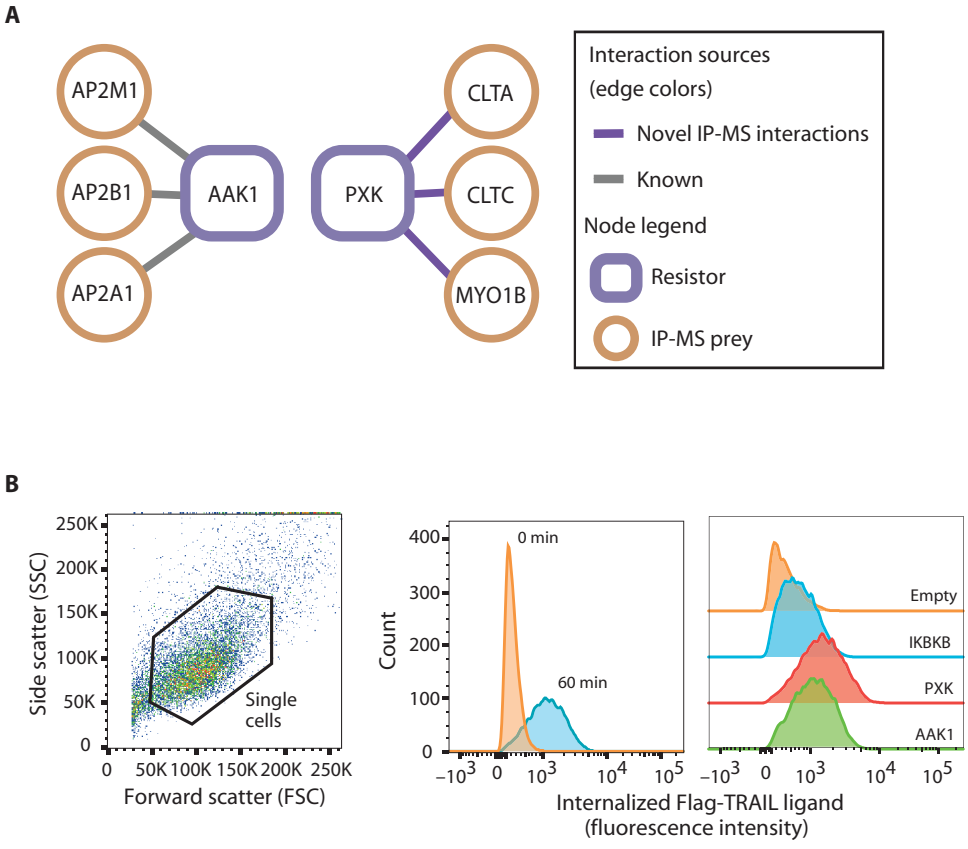

Fig. 4. Modulation of TRAIL endocytosis by AAK1 and PXK. (**A**) The interacting partners, as identified by IP-MS, of AAK1 and PXK that are associated with endocytosis. AAK1 interaction with the AP-2 complex was first reported in (*44*). (**B**) The endocytosis of FLAG-tagged TRAIL was measured by FACS in the specified cell lines. Presented are representative FACS analyses showing gating of the single-cell population (left panel), internalization of Flag-TRAIL at 0 and 60 min for the PXK cell line (center panel), and internalization at 60 min of empty vector, IKBKB, PXK, and AAK1 cell lines (right panel). (**C**) Quantification of the difference in internalization at 60 min of the four cell lines normalized to empty vector control (*$P < 0.05$, one-tailed Student's *t* test; error bars represent ±1 SD; $n = 3$).

Several of the phosphorylated sites that exhibited altered abundance after the cells were exposed to TRAIL have known regulatory roles, and by linking these sites to putative kinases, we can predict signaling events and how they provide protection or induction of apoptosis (Fig. 5). For instance, an activating phosphorylation site, Ser^{363}, on ribosomal protein S6 kinase 1 (RPS6KA1) (a resistor) (*52*), and an inhibitory phosphorylation site, Ser^{341}, on the RPS6K substrate TBC1 domain family member 4 (TBC1D4) (*53*) were decreased in cells exposed to TRAIL for 5 min and increased in cells exposed to TRAIL for 60 min (Fig. 5A). Phosphorylation of TBC1D4 at Ser^{341} provides a docking site for 14-3-3, thereby blocking TBC1D4's interaction with Rab proteins and increasing the transport of the glucose transporter GLUT4 to the plasma membrane (*53*). Increased GLUT4 on the cell surface may protect cells against glucose deprivation that can trigger apoptosis (*54*). Thus, this may reduce the cell's sensitivity to additional apoptotic signals, such as those mediated by TRAIL, thereby providing a potential mechanism by which RSP6KA1 functions as a resistor. However, this fails to explain the mechanism by which MAPK1 and MAPK3 function as sensitizers of TRAIL-induced apoptosis, which is likely mediated through other substrates.

An example of how dynamics of phosphorylation may provide putative inductive mechanisms is provided by examination of the dynamics of β-catenin (CTNNB1) and phosphatidylinositol 4-kinase β (PI4KB) (Fig. 5B). Phosphorylation of Ser^{191} of β-catenin was decreased at 60 min after TRAIL stimulation (fig. S10). Phosphorylation of this site by MAPK9 promotes β-catenin translocation into the nucleus and subsequent transcription of T cell factor (TCF)/lymphoid enhancer-binding (LEF)–regulated genes that promote cell survival (*55*). Therefore, decreased phosphorylation of CTNNB1 at this site is consistent with reports that TRAIL can inhibit WNT signaling to promote apoptosis (*56*). Similarly, PIK4B is predicted to be phosphorylated at Ser^{496} by cAMP-dependent protein kinase γ (PRKACG). When phosphorylated on Ser^{496}, PI4KB localizes to the nucleus where it converts phosphatidylinositol (PtdIns) to PtdIns4P (*57*). Decreased phosphorylation on PI4KB, as we detected at $t = 60$ min, would reduce the amount of PIK4B in the nucleus and the abundance of PtdIns4P. Low amounts of nuclear PtdIns4P and its higher phosphorylated derivatives are associated

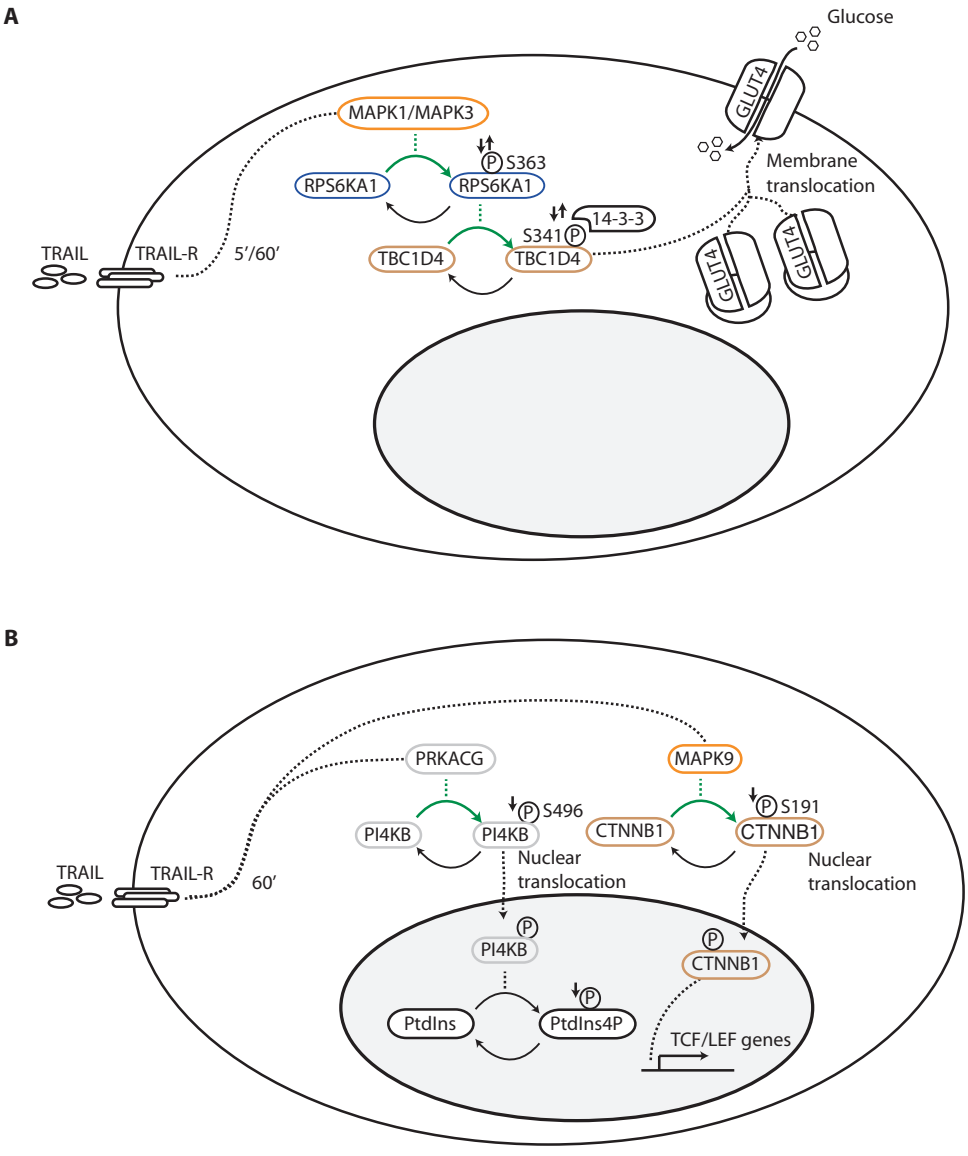

Fig. 5. Examples of regulatory phosphorylation events in the response to TRAIL. (A) Regulation of the abundance of the glucose transporter at the cell surface as a mechanism to resist apoptosis. Phosphorylation of Ser^{363} of RPS6KA1 and Ser^{341} of TBC1D4 changes dynamically in response to TRAIL: both are down after 5 min and up after 60 min (indicated by the up and down arrows, respectively). The increase in phosphorylation of these two proteins enables increased trafficking of the glucose transporter GLUT4 to the plasma membrane, which can protect cells from apoptotic stimuli. (B) Altered signaling through β-catenin and nuclear phosphoinositides as mechanisms for sensitization to apoptosis. Decreased phosphorylation on Ser^{496} of PI4KB reduces the amount of PIK4B in the nucleus and thereby reduces the amount of nuclear PtdIns4P, which is associated with increased cell death. Decreased phosphorylation of CTNNB1 (β-catenin) on Ser^{191} decreases the transcription of TCF/LEF-responsive genes that promote cell survival and proliferation. Color coding on proteins: orange, sensitizer; blue, resistor; gray, neutral; brown, modulated phosphorylated protein. The modulated phosphorylation event is depicted by a green arrow.

with increased cell death (*57*). In these examples, it is harder to reconcile the upstream kinases (MAPK9 and PRKACG) with a decrease in substrate phosphorylation except to state that it is consistent for a sensitizer MAPK9 to show decreased affinity for a site that would block apoptosis.

Network modeling predicts information flow from apoptosis-modifying kinases to modulated substrates

When we examined the predicted kinases from the global phosphorylation analysis, we found no significant enrichment of kinases identified as sensitizers or resistors (apoptosis-modifying) from our functional screens (distinct kinases for substrates significantly modulated by TRAIL: 56 neutral, 34 apoptosis-modifying; distinct kinase for substrates not significantly modulated by TRAIL: 57 neutral, 31 apoptosis-modifying; Fisher's exact test, $P = 0.757$). This suggested that the apoptosis-modifying kinases may affect TRAIL sensitivity indirectly by affecting the activity of other kinases. To predict whether apoptosis-modifying kinases exerted influence indirectly through other kinases, we used computational modeling to study the flow of "information" between kinases and from kinases to substrates that showed significantly different phosphorylation abundance in cells exposed to TRAIL (herein referred to as modulated substrates). To start this analysis, we created a kinase interaction network from the expanded IP-MS network that includes predicted kinase-substrate pairs (1779 edges), predicted kinase-substrate pairs from the global phosphorylation analysis for modulated substrates (347 edges), and 469 pairs imported from external sources (literature, public databases) to connect apoptosis-modifying kinases that were unlinked without these pairs. Combined, this kinase interaction network contained 2595 edges (table S8). The dynamic information regarding the edges obtained from the TRAIL time course phosphoproteomics analysis enabled the generation of three subnetworks, each representing a time point of TRAIL stimulation ($t = 0$, 5, or 60 min) (table S8). We only added a kinase-modulated substrate edge to a subnetwork if the phosphorylated site on the substrate was significantly increased at that time point relative to another time point (for example, if a phosphorylated site was increased at t_5/t_0, the edge was only added to the $t = 5$ network; conversely, if it was decreased at t_5/t_0, it was only added to the $t = 0$ network). We included the static interactions from the IP-MS (including the predicted kinase-substrate pairs from the expanded network) and the external data sets in all three subnetworks.

We assigned interaction probabilities to all edges in these networks (table S8, see Materials and Methods) and used these probabilities to calculate the flow of information from one kinase (source) to another kinase or modulated substrate (sink) within each subnetwork (Fig. 6A). The flow

for each edge is considered unidirectional from kinase to substrate for pairs predicted from phosphoproteins and bidirectional for all other pairs. We combined the probabilities of each edge along a maximum of 10 distinct paths from source to sink to determine one information flow (I_f) value for each source/sink pair for each TRAIL stimulation time point (table S9, see Materials and Methods). The change in information flow (ΔI_f) between the subnetworks for each source/sink pair was then calculated (that is the I_f at $t = 0$ min for each pair was subtracted from its I_f value at $t = 5$ min to generate one matrix and from its I_f value at $t = 60$ min to generate a second matrix) (table S9). To test if pairs with apoptosis-modifying kinases as the sources have increased ΔI_f compared to pairs with neutral kinases as the sources, we performed Fisher's exact tests at different quantile values for sources and sinks (fig. S13), and found a significant enrichment for apoptosis-modifying kinases at high ΔI_f values (>0.5 to <0.95), consistent with the tight relationship between kinases that influence DLD-1 cells' sensitivity to TRAIL and the phosphoproteins affected by TRAIL.

To examine the relationship between kinase (source) and modulated substrate (sink) pairs with high ΔI_f, we performed hierarchical clustering on the ΔI_f values for the $t_5 - t_0$ network (93% quantile; Fig. 6B). PXK, which promoted endocytosis of the TRAIL receptor (Fig. 4B), was one of the kinase sources identified with increased ΔI_f to its sinks. The kinases LIMK2, IRAK1, ARAF, and ILK that we identified as highly connected in our IP-MS network (Fig. 3B) clustered together in this matrix. In general, modulated substrates that showed decreased phosphorylation at $t = 5$ min (table S7) overall had negative ΔI_f, and modulated substrates with increased phosphorylation at $t = 5$ min had positive ΔI_f (table S9). This is not unexpected because only edges that had different probability scores between time points contributed to ΔI_f values (for example, I_{K1} to $Sink_1$ in Fig. 6A). The calculated routes from source to sink may have had no differential edges (for example, the route through I_{P2} to $Sink_1$), one differential edge contributing to the ΔI_f value (for example, through I_{P1} to I_{K1} to $Sink_1$), or multiple differential edges (for example, through I_{P3} to I_{K1} to $Sink_1$). Most of the network was composed of static edges derived from the IP-MS data set, which had the same I_f values for all time points, and did not contribute to ΔI_f values. As a result, the final edge leading to a modulated substrate sink tended to dominate the ΔI_f value. Checkpoint kinase 2 (CHEK2) was only linked to the kinase interaction network through retinoblastoma 1 (RB1), which had decreased phosphorylation at $t = 5$ min, and thus displayed negative ΔI_f values relative to the other kinase sources shown in Fig. 6B.

Notwithstanding the biased contributions of the final edges to modulated substrates, this analysis identified which apoptosis-modifying kinases were closely linked in network space to substrates modulated by TRAIL. Cell division cycle 25B (CDC25B) was the recipient of the highest positive ΔI_f at the 5-min stimulation time (Fig. 6B). The site that we identified as modulated by TRAIL, Ser^{375} (increased in phosphorylation at $t = 5$ min compared to $t = 60$ min, table S7), is bound by 14-3-3 proteins when phosphorylated (*58*), which prevents CDC25B from activating CDKs by dephosphorylating inhibitory residues (*59*). Selected routes from the five apoptosis-modifying kinase sources (WEE1, ILK, ABL1, STK32B, and DAPK1) with the highest ΔI_f values from the 93% quantile to CDC25B are shown in Fig. 6C. None of these kinases were directly linked to CDC25B, but they were all within a closely connected network that may influence MAPK-activated protein kinase 2 (MAPKAPK2) that was predicted to phosphorylate CDC25B. RB1 was the recipient of the highest negative ΔI_f in Fig. 6B. Phosphorylation of Ser^{612} was decreased at 5 min after TRAIL treatment (compared to $t = 0$ min) and increased at 60 min (relative to $t = 5$ min) (table S7). Because phosphorylation of RB1 on Ser^{612} is essential for cell survival and its anti-apoptotic activity (*60*), the decrease at $t = 5$ min may represent a proapoptotic signal. The top five apoptosis-modifying kinase sources (ABL1, LIMK2, IRAK1, FES, and WEE1) with the highest ΔI_f values from the 93% quantile were linked to RB1 through multiple routes that traveled through CHEK1 and CDKs (Fig. 6C).

We made similar connections between kinase sources and modulated substrates in the $t_{60} - t_0$ hierarchical cluster of ΔI_f values at the 93% quantile (fig. S14A). Stathmin 1 (STMN1) was the recipient of the highest positive ΔI_f. Phosphorylation on STMN1 at Ser^{25} was increased at 60 min after TRAIL treatment (table S7). Ser^{25} of STMN1 is phosphorylated after TNF stimulation, and this phosphorylation may play a minor role in inhibiting STMN1's ability to destabilize microtubules thus leading to cell death (*61*). The top five apoptosis-modifying kinase sources (ARAF, ILK, WEE1, MAPK3, and ABL1) with the highest ΔI_f values from the 93% quantile were connected through CDK1 and MAPK3 to STMN1 (fig. S14B). These examples illustrate the value of information flow analysis to identify the close connections between apoptosis-modifying kinases and modulated substrates with key regulatory roles in apoptotic or other regulatory processes. We suggest that the apoptosis-modifying kinases from the 93% quantile and in particular those [WEE1, PXK, IRAK1, DAPK1, ARAF, ILK, CSNK2A1, protein kinase Cα (PRKCA), ABL1, and PRKCZ] identified in both matrices (Fig. 6B and fig. S14A) be further investigated as possible candidates for combination therapy.

DISCUSSION

Cancer chemotherapy is a race against the emergence of resistant cells. Initial results from clinical studies with TRAIL or its receptor agonists prove that, so far, these treatments are no exception to this issue. Like most other targeted therapeutics, attention has now turned to identifying targets that can be inhibited in combination with TRAIL to promote tumor cell apoptosis (*5*). Here, we focused on protein kinases because they are druggable and regulate virtually all cellular processes, including apoptosis. Through modulation of kinase abundance by overexpression and depletion studies, we identified 169 kinases that affected TRAIL signaling, of which 109 inhibited apoptosis (resistors). The apoptosis-modifying kinases are spread throughout the kinome with little bias among kinase subfamilies (fig. S5). An exception might be the MAPK family; members tended to promote apoptosis in our screens, which may result from DLD-1 cells having an activated K-Ras that sensitizes the cells to TRAIL (*62*).

Compared to other siRNA screens involving TRAIL (*63*–*65*), we had a higher hit rate (35% compared to 2 to 8%), suggesting that our screen was more sensitive and less prone to false negatives. Of the hits in common between the screens, we found that 32, 56, or 36% of the kinases that we identified as apoptosis modifiers matched those identified in screens of breast cancer MDA-MB-453 (*63*), cervical cancer HeLa (*64*), or glioblastoma U251MG (*65*) cell lines, respectively. Proteins that did not match presumably reflect differences in the experimental assays used, cell context, and the selection of significance cutoff limits that would affect false-positive and false-negative rates. Even with our higher hit rate, there are some obvious TRAIL-influencing kinases that were not identified in our screens. For instance, members of the AKT family had no impact on TRAIL signaling when depleted and AKT1 was neutral when overexpressed.

The overlap of apoptosis-modifying kinases identified between the two siRNA and overexpression data sets was not very large (Table 1), in part because the siRNA screen was more extensive than the overexpression screen. We expect that expanding the latter assay to include all protein kinases would increase this overlap. Further validation of all knockdown hits with orthogonal approaches would reduce the number of false positives. Because seven of eight kinase hits were reproduced in a small-scale validation, we anticipate that the rate of false positives may not be particularly high.

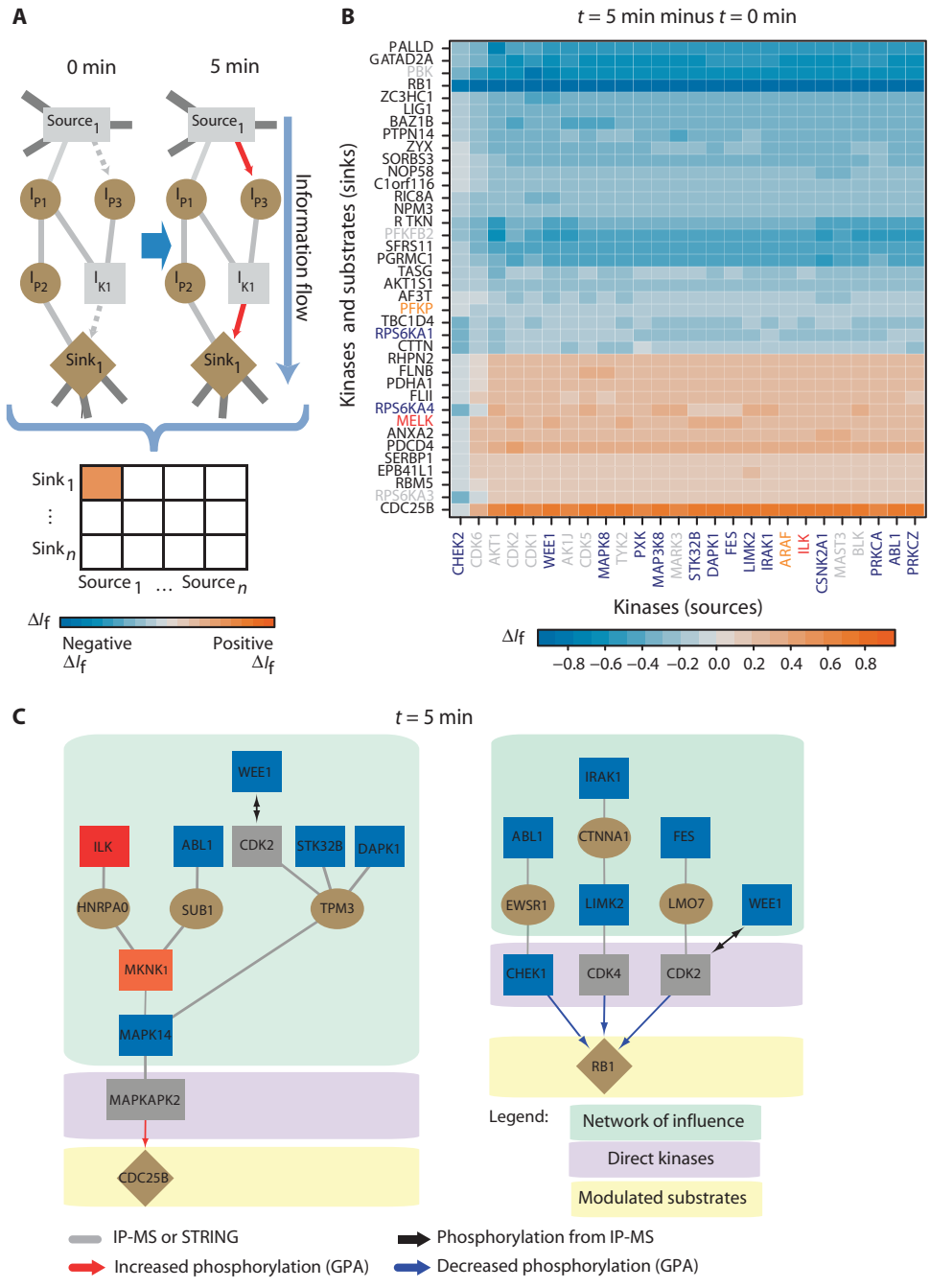

Fig. 6. Information flow analysis identifies connections between apoptosis-modifying kinases and substrates that exhibit significant changes in phosphorylation state in response to TRAIL. (**A**) A diagram illustrating how the information flow between kinases or between a kinase and a modulated substrate may change upon TRAIL stimulation. Optimal paths connect every source (kinase, source of information flow) with every sink (another kinase or modulated substrate, recipient of information flow). An edge in the network for a modulated substrate-kinase pair is only added at the time point with increased phosphorylation of the substrate (red solid arrows at the $t = 5$ min time point). Up to a maximum of 10 independent pathways for each source/sink pair were combined to generate an Information flow value (I_f). The resulting value for each pair at $t = 0$ was then subtracted from the values calculated for networks generated at $t = 5$ or $t = 60$ min after TRAIL. In this example, because of two phosphorylated sites (I_{P3} and $Sink_1$) with increased phosphorylation at $t = 5$ min (red arrows), there is a positive change in information flow (ΔI_f) recorded for the $Source_1$ to $Sink_1$ pair at $t = 5$ min. A matrix containing ΔI_f values for all source to sink combinations is presented in table S9. I_p, intermediate protein; I_k, intermediate kinase. (**B**) A cluster illustrating significant ΔI_f (at the 93% quantile) between pairs from $t = 0$ to $t = 5$ min TRAIL stimulation (hierarchical clustering, distance: Euclidean, method: complete). (**C**) Selected routes from the top five apoptosis-modifying kinase sources (WEE1, ILK, ABL1, STK32B, and DAPK1 for CDC25B; IRAK1, ABL1, FES, LIMK2, and WEE1 for RB1) with the highest ΔI_f at the 93% quantile for the $t = 5$ min minus $t = 0$ min matrix to the indicated sinks. GPA, global phosphorylation analysis.

Although both screens reported similar number of sensitizers (11% for siRNA and 6% for overexpression), the overexpression screen identified 29% more resistors than the siRNA screen. This increase may have resulted from the long-term expression of the kinases in these cells that forced the cells into a new state that was less responsive to TRAIL. Notwithstanding these concerns, the low overlap between the two methods also points to their fundamental differences and how they can complement one another. For instance, depending on the amount of endogenous protein, the cell may be more affected by overexpression if the kinase is normally limiting or absent and, conversely, more affected by decreased abundance if the kinase is normally in excess. Overexpression also avoids the issue of siRNA off-target effects and may circumvent isoform redundancy. However, overexpression may not correlate with increased kinase activity, especially in kinases that require activating phosphorylation or the presence of other proteins for activity. Furthermore, the amounts of ectopically expressed proteins are often many fold above endogenous and, therefore, may lead to the formation of aberrant interactions. Thus, by using both siRNA-mediated knockdown and overexpression, we mitigated the negative aspects of each screen individually and identified 169 candidates for further study.

Many of the kinases that we identified as apoptosis-modifying here have previously been identified as regulating apoptosis, although not

necessarily in TRAIL-induced cell death. Several of these, such as ILK, PRKDC (*66–69*), and MAPK1 and MAPK3 (*62, 70*), had conflicting reports in the literature regarding to their roles in apoptosis. ILK, for instance, can act as an oncogene or tumor suppressor depending on cellular context (*71*), and it can activate not only antiapoptotic pathways through AKT but also proapoptotic pathways by interacting with CASP8 or CASP9 (*72*). This is not surprising because kinases are often integrators of signals originating from multiple input cues, and the outcome of their activity is context-dependent or multivariate. For example, MAPK8, also known as JNK1, can be proapoptotic, antiapoptotic, or even neutral depending on the concentrations of TNFα and EGF that were applied to the cells (*73*). IKBKB, which activates NF-κB, had a consistent phenotype as a resistor in both the siRNA and overexpression screens. In contrast, IRAK4, an activator of nuclear factor κB (NF-κB) in the context of innate immunity (*74, 75*), was the most potent resistor to apoptosis when overexpressed, but it also promoted resistance when depleted. This discordance led IRAK4 to be classified as a modulator similar to ILK. Given that NF-κB can be both pro- and antiapoptotic (*76*), perhaps it is not surprising that an upstream activator's response can vary. With these and other examples, we see that kinases function as pro- or antiapoptotic depending on the cellular context.

DLD-1 cells are a colorectal adenocarcinoma cell line characterized by a *KRAS* allele that produces constitutively active KRAS and mutated *APC*, the latter of which increases the abundance of β-catenin. As a consequence of the activated KRAS, the cells are sensitized to TRAIL, owing in part to increased surface abundance of TRAIL receptors (*62*). Consistent with this characteristic of DLD-1 cells, knockdown of the kinases MAPK1 and MAPK3, which are activated downstream of KRAS, decreased CASP3 cleavage of the EC-RP reporter even though these kinases are more often viewed as promoters of cell survival. β-Catenin, a downstream effector of WNT signaling that activates antiapoptotic genes (*55*) and a substrate of CASP3 and CASP8 (*77*), was connected to several apoptosis-modifying kinases in our interaction network, and a regulatory phosphorylation site on β-catenin showed decreased phosphorylation upon TRAIL stimulation. Presumably, to trigger apoptosis, the cell needs to attenuate the WNT signal, and our network analysis suggested that this may be accomplished through regulation of β-catenin.

Integrating data between the phenotypic (siRNA and overexpression) and proteomic (IP-MS and phosphoproteomic) screens identified two kinases of particular interest: PXK and AAK1. Both were classified as resistors in both the loss-of-function and gain-of-function screens. The IP-MS screen identified partners linked to endocytosis for these kinases, confirming previous reports that they play a role in this process (*43–45*). Endocytosis of TRAIL receptors occurs through a clathrin-dependent pathway, similar to receptor tyrosine kinases (RTKs), in which c-CBL mediates the monoubiquitination of the intracellular region of the receptor, leading to their recognition by the endocytosis machinery and then degradation to down-regulate TRAIL responsiveness (*78–80*). Oncogenic inhibition of c-CBL ubiquitination promotes tumorigenesis through increased RTK surface residency and growth factor signaling (*81*). However, this mechanism may also leave the cell more susceptible to TRAIL-induced apoptosis. Indeed, the TRAIL response depends on the amount of TRAIL receptor at the cell surface, because blocking the transport of TRAIL receptors to the plasma membrane or increasing their endocytosis leads to TRAIL resistance (*79, 82*). We found that overexpression of AAK1 or PXK increased the uptake of TRAIL, indicating increased endocytosis of TRAIL receptors. This analysis suggests that blocking receptor endocytosis through AAK1 or PXK inhibition may be one strategy to promote TRAIL sensitivity in tumors provided that the commensurate increase in growth receptors does not negate the benefit.

PXK was also identified as a kinase with high ΔI_f to modulated substrates. Information flow is a measure of degree of influence that can be transmitted from one node to another within a network. Here, we showed that apoptosis-modifying kinases are more likely to have increased ΔI_f to each other and to substrates that exhibited TRAIL-regulated changes in phosphorylation. Previous studies have used publicly available protein-protein interaction databases to predict previously unknown gene-phenotype associations, and this revealed that mutations in genes encoding interacting proteins lead to similar disease phenotypes (*83, 84*). Vanunu *et al.* (*85*) used the concept of information flow to propagate from known disease genes, through a protein-protein interaction network, to infer disease-causing complexes. Here, we extended this concept using measurements in the same cell line, specifically focusing on differential changes in network connectivity associated with TRAIL stimulation. In the future, this analysis could be improved by the addition of more dynamic edges through IP-MS for more kinases and at different TRAIL time points as well as by additional phosphoproteomics analysis. However, even with the current information flow analysis, we identified apoptosis-modifying kinases connected to TRAIL-responsive phosphoproteins. In addition to PXK, we identified 18 other apoptosis-modifying kinases (by combining results at 93% quantile for the $t_5 - t_0$ and $t_{60} - t_0$ clusters), of which 10 were common to both clusters: resistors [PXK; WEE1, the negative regulator of CDK2 (*86*); IRAK1, a positive regulator of innate immunity downstream of the interleukin and toll receptors (*87*); PRKCZ, an atypical protein kinase C linked to cell polarity (*88*) that when inactivated impairs NF-κB signaling in mice (*89*); CSNK2A1, a known inhibitor of apoptosis that phosphorylates caspase recognition motifs (*36*); DAPK1, a tumor suppressor identified as an inducer of cell death that may suppress cell death in certain contexts (*90, 91*); PRKCA, a member of the protein kinase C family that has been shown to inhibit TRAIL-induced apoptosis in the Jurkat T cell line (*92*); ABL1, encoded by a proto-oncogene that when persistently inhibited can sensitize cells to TRAIL (*93*)], modulator ILK, and sensitizer ARAF that as a downstream target of activated K-Ras may contribute to the sensitivity of DLD-1 cells to TRAIL (*62*). Future combinatorial studies of these ten kinases with compounds that target resistors for inhibition and sensitizers for activation in conjunction with TRAIL and with each other would further validate these potential targets.

In summary, we have conducted a series of complementary screens to identify 169 kinases that influence TRAIL responsiveness and to identify regulatory interaction networks containing these kinases. Within these networks, we used information flow analysis to show that kinase nodes exhibiting the greatest amount of change in connectivity in cells exposed to TRAIL are more likely to modify TRAIL-induced apoptosis. We used this information flow analysis to reduce the list of 169 potential apoptosis-modifying kinases for combination treatment to a more manageable number of 10 kinases tightly connected to modulated substrates at both 5 and 60 min after TRAIL stimulation. Because these kinases are likely to have central roles in controlling the cellular response to apoptotic stimuli, we suggest they may represent fragile nodes and warrant further investigation in a combinatorial manner as sensitizers to TRAIL.

An online resource of our study is presented at http://pawsonlab.mshri.on.ca/KinaseTrail/ and data from this site is available in files S1 to S7.

MATERIALS AND METHODS

Cloning

A detailed cloning summary is provided in table S2 and includes acknowledgments of clones from external sources (*94–97*) and details regarding the parent vectors. To create gateway entry clones, open reading frames

(ORFs) were amplified by polymerase chain reaction (PCR) from the templates indicated in table S2 using Phusion DNA polymerase (NEB) with Gateway-compatible sequences appended to the end of the primers (5′ sequence: ggggacaactttgtacaaaaaagttggcacc; 3′ sequence: ggggacaactttgtacaagaaagttgggta). The resulting products were then cloned into pDONR223 (*94*) using BP clonase (Invitrogen) and subsequently into Gateway destination vectors using LR Clonase (Invitrogen) according to the manufacturer's protocols. All inserts were sequence-verified using CodonCode Aligner software. Clones were tracked in OpenFreezer (*98*).

Cell culture and creation of stable cell lines

DLD-1 (ATCC CCL-221) and DLD-1 LacZeo/TO [compatible with Invitrogen's FlpIN T-Rex system (*99*)] cells were propagated in RPMI medium plus 10% fetal bovine serum (FBS). Human embryonic kidney (HEK) 293T cells were propagated in Dulbecco's modified Eagle's medium plus 10% FBS. Kinases in the V2972 Triple FLAG vector (table S2) were transfected into DLD-1 cells using Lipofectamine 2000 (Invitrogen), and stably transfected cells were selected using puromycin (2.5 μg/ml). Pools of puromycin-resistant cells were then sorted by FACS on a MoFlo (DAKO) to select for cells with high green fluorescent protein (GFP) expression because V2972 contains an internal ribosome entry site (IRES)–GFP segment. For cloning into DLD-1 LacZeo/TO cells, V4869-based vectors were transfected using Lipofectamine 2000 and placed under hygromycin (200 μg/ml) selection to obtain pools of stably transfected cells. DLD-1 cells were transfected with the pECFP-DEVDR-Venus plasmid using Lipofectamine 2000 and selected using G418 (2 μg/ml). The pool of resistant cells was then FACS-sorted for high expression using a MoFlo.

Immunoblotting

Cells were lysed in lysis buffer [LB; 50 mM Hepes (pH 8.0), 100 mM KCl, 2 mM EDTA, 10% glycerol, 0.5% NP40, 50 mM NaF, 50 mM β-glycerol-phosphate, supplemented with aprotinin (10 μg/ml), leupeptin (10 μg/ml), 1 mM $NaVO_4$, 1 mM phenylmethylsulfonyl fluoride, 1 mM dithiothreitol (DTT), 0.1 mM okadaic acid], and lysates were clarified by centrifugation at 20,000*g* for 30 min. The resulting supernatant was resolved by SDS–polyacrylamide gel electrophoresis (SDS-PAGE) and transferred onto FluoroTrans (Pall) membranes. The blots were probed with primary antibodies at 1:1000 unless specified: FLAG M2 antibody (1 μg/ml, Sigma, cat#F1804), GFP antibody (1:5000, Abcam, cat#ab290), GAPDH antibody (Santa Cruz Biotechnology, cat#sc-25778), α-tubulin antibody (1:5000, Sigma, cat#T9026), RSK1 antibody (Upstate, cat#06-668), RSK pT359 and pS363 antibody (Cell Signaling, cat#9344), glycogen synthase kinase 3A (GSK3A) antibody (Cell Signaling, cat#4337), GSK3A and GSK3B pY279 and pY216 antibody (Santa Cruz Biotechnology, cat#sc-11758), CTNNB1 antibody (1:500, Santa Cruz Biotechnology, cat#sc-7199), CTNNB1 pS675 antibody (Cell Signaling, cat#4176), signal transducer and activator of transcription 3 (STAT3) antibody (1:500, Santa Cruz Biotechnology, cat#sc-482), STAT3 pS727 antibody (BD Biosciences, cat#612542), CDC2 antibody (Cell Signaling, cat#9112), CDC2 pT161 antibody (Cell Signaling, cat#9114), TRAIL-R1 antibody (Pierce, cat#MA1-41076), and TRAIL-R2 antibody (Pierce, cat#MA1-19416). The blots were then probed with secondary antibodies: 1:15,000 goat anti-mouse IR680 (Mandel, cat#LIC-926-68020) or 1:15,000 goat anti-rabbit IR800 (Mandel, cat#LIC-926-32211). IRDye-conjugated secondary antibodies were visualized, and bands were quantified using a LiCor Odyssey.

RNAi screen

DLD-1 cells (~10^5) stably expressing the EC-RP plasmid were seeded onto Opti-Clear 96-well assay plates (BD Falcon) containing preformed siRNA/liposome complexes [30 nM each of a siGenome Smart-Pool from the Protein Kinase set (Thermo Scientific) and 0.3 μl of Lipofectamine RNAiMax (Invitrogen)]. siRNA transfection and cell seeding were performed using the Beckman Coulter Biomek FX liquid handling robot. After 48 hours, the cells were serum-starved (RPMI with 0.1% FBS) overnight, washed with phosphate-buffered saline (PBS), and stimulated with TRAIL (100 ng/ml in RPMI, 0.1% FBS, without phenol red). At the time points indicated, the intensities parallel and perpendicular to the excitation polarization were measured for each well using the Analyst (Molecular Devices) microplate reader with excitation filter: 425/35 nm, emission filter: 530/25 nm, and dichroic: 505 nm.

Data output from the Analyst software was uploaded into CoreFlow, a workflow management system (*100*). Fluorescence polarization (FP) was derived from the parallel ($I_{||}$) and perpendicular ($I_{\perp}$) intensities using the following equation:

$$\mathrm{FP} = \frac{I_{||} - I_{\perp}}{I_{||} + I_{\perp}}$$

The screen was performed in duplicate with two technical replicates for each biological replicate for an average of four replicates per gene. To identify any outlying replicates because of low reporter signal, we took the median value of the intensity parallel of the five time points for each replicate and looked at the global distribution of these values. Any replicates with a median value less than the 13% quantile were eliminated. Each replicate was then normalized by subtracting its signal at $t = 0$ hour TRAIL stimulation. Median time profiles for each gene were classified by hierarchical clustering (distance: Euclidean, method: complete) and separated into three main groups: "resistors," "sensitizers," and "neutrals." All statistical analysis and visualization were performed in R. For comparison to GO annotation, GO terms for the relevant kinases were downloaded from Ensembl BioMart (www.ensembl.org/biomart/martview), and kinases with a GO term that included "apoptosis" or "apoptotic" were scored as apoptotic kinases.

PI staining

Cells were seeded in 96-well plates (Sarstedt) and serum-starved overnight (RPMI with 0.1% FBS). After treatment with TRAIL (100 ng/ml) for 4 hours, the medium was collected in a 96-well, V-bottomed plate (Corning Costar) along with the cells, which were trypsinized, fixed in ice-cold ethanol (70%), and stored at −20°C. Upon thawing, the cells were centrifuged at 2655*g* for 2 min, washed with PBS, and then incubated with PI/ribonuclease stain buffer (BD Pharmingen) for 1 hour before FACS analysis on an LSRFortessa (BD Biosciences). The sub-G_1/G_0 cell population was counted as a proportion of the total single-cell population, representing DNA fragmentation in the nucleus during apoptosis.

Overexpression screen and FACS analysis

Cell lines were thawed from liquid nitrogen and passaged twice in RPMI medium containing puromycin (2 μg/ml) before seeding in six-well plates. After 24 hours, cells were serum-starved in RPMI with 0.1% FBS overnight. Cells were then stimulated with recombinant TRAIL (100 ng/ml) (*101*) in RPMI with 0.1% FBS. At the indicated time points, cells were trypsinized and transferred to a 1.5-ml microcentrifuge tube in ice-cold RPMI with 10% FBS. Cells were then incubated with BD Cytofix (Becton-Dickson) at 37°C (15 min, with shaking at 750 rpm) and then placed in a U-bottomed 96-well plate. The cells were then incubated with BD Perm Buffer III for 1 hour at 4°C, blocked with tris-buffered saline with 0.05% Tween 20 (TBST) containing 2% FBS for 1 hour, and washed three times with TBST before incubation with primary rabbit antibody recognizing

cleaved CASP3 (BD Biosciences, cat#559565) at 1:300 dilution overnight at 4°C. After being washed three times with TBST, the cells were incubated with goat anti-rabbit secondary antibody conjugated to Alexa 647 (Life Technologies, cat#A-21244) at 1:300 dilution along with primary mouse antibody conjugated to phycoerythrin that recognized cleaved PARP (BD Biosciences, cat#552933) at 1:5 dilution. After being washed three times with TBST, the samples were resuspended in TBST, and fluorescence was measured using FACSArray (BD Biosciences).

Gating was performed using the FlowJo software (Tree Star) to first identify the single-cell population and then to segregate cells on the basis of cleaved CASP3 and cleaved PARP intensities. Cells were gated to distinguish the single-cell population with high cleaved CASP3 and high cleaved PARP from low cleaved CASP3 and low cleaved PARP (fig. S4). Percent apoptosis is defined as the percentage of cells in the single-cell population with high cleaved CASP3 and high cleaved PARP over the total number of cells. For the 2- and 4-hour time points, percent apoptosis was normalized by subtracting the value at $t = 0$ hour for each sample. To control for variations between batches, all samples within a batch were normalized to two controls present in the batch (DLD-1 stable cell lines expressing either CSNK2A1 or empty vector): For each time point, the average of the median values of each control was subtracted from the sample. Hotelling's T^2 test for multivariate (two-dimensional) P value significance was performed with the R package "ICSNP" by comparing data from each overexpressed kinase to controls and to all other genes. A kinase was assigned to the same phenotype as a control if its P value compared to that control was >0.5 or if the $\log_2$ value of the highest P value compared to a control/over the next highest P value was >128 (fig. S4). Any kinase (with the exception of IRAK4, which was manually assigned a phenotype) that did not fit either of these two conditions was considered "unclassified." All data and analysis scripts are stored in CoreFlow. Visualization of raw BD FACSArray data was performed in R with the bioconductor, prada, lattice, and hexbin packages.

Immunoprecipitation-MS

Cells at ~90% confluency (~2×10^8) were washed in PBS (pH 7.4) and lysed by incubation for 5 min at 4°C in 7.5 ml of LB buffer. The lysate was clarified by centrifugation at 20,000*g* for 30 min, and added to 150 µl of packed Sepharose 4B 200 beads (Sigma) for 1 hour at 4°C to preclear the lysate. The beads were pelleted by centrifugation at 2000*g* for 30 s, and the lysate was then added to 30 µl of packed FLAG M2 antibody–linked agarose beads (Sigma, cat#A2220) and rotated for 3 hours at 4°C. The beads were then washed four times in LB buffer and four times in LB2 buffer (LB buffer minus glycerol, NP40, and NaF). Finally, protein was eluted from the beads by incubation with 2% formic acid. Samples were processed using a solid-phase digest protocol as previously described (*102*). Briefly, columns were made with 200-µm (internal diameter) fused-silica tubing and packed with 3 cm of PolySulfoethyl A beads (particle size, 12 µm; pore size, 300 Å) (Western Analytical) using a pressure bomb (nitrogen gas, 100 to 500 psi). Protein eluates were loaded on the column and washed with 10 mM potassium phosphate buffer (pH 3) followed by high-performance liquid chromatography (HPLC)–grade water. Bound proteins were reduced in DTT solution (100 mM DTT/10 mM NH_4HCO_3, pH 8) for 30 min and washed with HPLC-grade water. Reduced proteins were alkylated and trypsin-digested for 1 to 2 hours in trypsin solution [sequencing-grade porcine trypsin (2 mg/ml; Promega)/100 mM tris/10 mM iodoacetamide (pH 8)]. Peptides were eluted in 15 µl of 200 µM NH_4HCO_3 (pH 8), and 1 µl of 50% formic acid was added to a final volume of 16 µl. Samples were analyzed on a QSTAR Elite QqTOF mass spectrometer equipped with a nanospray III ion source (AB SCIEX) and coupled to a 1D+ Nano LC (Eksigent) as previously described (*102*). Samples were injected directly onto a column packed in-house (75-µm inner diameter) with 3.5-µm Zorbax C-18 (Agilent) and analyzed using a 90-min gradient from 5 to 30% solvent B (solvent A: 0.1% formic acid in water; solvent B: 0.1% formic acid in acetonitrile) at a flow rate of 250 nl/min.

MS identification and filtering

Tandem mass spectra were extracted, charge state deconvoluted, and deisotoped in Analyst version 2.0. Wiff files were converted to .mgf format using ProteinPilot software, and both formats were stored in ProHits (*103*). All tandem mass spectra were analyzed using Mascot (Matrix Science) version 2.2 against the human Ensembl database (release 50 supplemented with entries from the cRAP database version 2009.05.01, from GPM and GFP sequences—a total of 46768 sequences; 24060923 residues). Trypsin was chosen for digestion with up to two missed cleavages. Carbamidomethyl (C) was set as a fixed modification, and deamidated (NQ), pyro-Glu (N-term Q), pyro-Glu (N-term E), oxidation (M), phosphoTyr, and phosphoSer/Thr were set as variable modifications. ESI-QUAD-Tof type fragmentation was selected with peptide mass tolerance set to 70 parts per million (ppm), and fragment mass tolerance set to 0.15 dalton. All Mascot results for the same bait in the same backbone vector were combined together and analyzed in Scaffold (Proteome Software Inc.). Proteins with at least two peptides and a protein probability of greater than 80% as assigned by Scaffold were retained for further analysis. Any protein that was identified as a prey for more than one control sample (empty vector or GFP) or was above our high frequency cutoff [prey present in >19 N-terminal FLAG-tagged bait immunoprecipitates or >5 C-terminal FLAG-tagged bait (fig. S7) immunoprecipitates] was removed. We also further refined prey frequency by assigning a "very high" stringency to those prey whose frequency was <10 or <4. All remaining preys were then compared to these high-frequency proteins. If a protein had no unique peptides compared to high-frequency proteins, then it was removed from the prey list and placed on the high-frequency list. To remove bait carryover contamination, any kinase that was identified as a prey of another kinase was removed if the digests were performed within a few days of each other or if the prey was a bait within a preceding MS sample. Finally, any prey from the C terminus–tagged kinase experiments that was identified as a high-frequency prey in the N terminus–tagged kinase set was also removed. Phosphopeptides were analyzed by the A-score algorithm (*104*) within Scaffold PTM (Proteome Software Inc.). Any phosphosite with an A-score of 20 or higher (a "high-confidence" phosphosite) was then analyzed by NetPhorest (*47*) and an updated version of NetworKIN (*51*) algorithms (score cutoff of 0.035 for each; only kinases whose NetworKIN score was within 10% of the top scoring kinases were retained).

Coimmunoprecipitation validation

HEK293T cells were transfected with 1 µg of each plasmid using Lipofectamine 2000. Two days after transfection, the cells were lysed in LB buffer, and the lysates were clarified by centrifugation at 20,000*g* for 30 min before incubation with 2.5 µl of packed FLAG M2 antibody–linked agarose (Sigma, cat#A2220) or 2 µl of GFP antibody (Abcam, cat#ab290) bound to protein A–Sepharose. The beads were washed in LB buffer and boiled in 2× SDS sample buffer before resolution on polyacrylamide gels and immunoblotting.

Phosphoproteomics

SILAC labeling and phosphopeptide enrichment protocols were adapted from (*105–107*). Isotopomeric version of arginine and lysine ("heavy" C13N15, "medium" C12N15, and "light" C12N14, respectively) were purchased from Sigma Isotech. SILAC media were prepared using RPMI

deficient in arginine and lysine (Caisson Lab), 10% dialyzed FBS (Gibco), penicillin/streptomycin (Gibco), and arginine and lysine (50 mg/liter). DLD-1 cells were passaged a minimum of eight times in SILAC media to ensure maximal labeling, before seeding in 500-cm^2 tissue-culture plates (Corning). The cells were then serum-starved overnight (SILAC media with 0.1% dialyzed FBS) followed by stimulation with TRAIL (200 ng/ml) for 5 or 60 min and harvesting in 9 M urea lysis buffer [9 M urea, 20 mM Hepes (pH 8), 1 mM Na_3VO_4, 2.5 mM NaPPi]. A fraction of each lysate was resolved by SDS-PAGE; bands were excised, digested with trypsin, and analyzed on an LTQ Orbitrap (Thermo Fisher Scientific) as described above to identify nonphosphorylated peptides to be used for normalization of protein abundance. The remaining cell lysates were sonicated (3 × 30 s at 15 W), centrifuged (20,000*g* for 30 min), reduced (100 mM DTT), alkylated (10 mM iodoacetamide), and digested with trypsin (Warrington, 1:100 enzyme/substrate ratio) at room temperature overnight. Digested lysates were acidified [1% trifluoroacetic acid (TFA), final concentration], and peptides were purified on C18 SepPak columns (Waters), dried, and stored at –80°C. Peptides were resuspended in 25% acetonitrile/0.1% TFA, and pH was adjusted to 2.5. PhosSelect (Sigma) was prepared in parallel by washing first in 0.1% TFA and then twice in 25% acetonitrile/0.1% TFA, before being incubated with the resuspended peptides (2 mg peptide/300 µl PhosSelect) in a final volume of 250-µl 25% acetonitrile/0.1% TFA for 2 hours at room temperature with rotation. Beads were subsequently washed twice in 800 µl of 0.1% TFA, twice in 800 µl of 50% acetonitrile/0.1%TFA, and once in 800 µl of water. Peptides were eluted with 350 µl of 100 mM ammonium bicarbonate (pH 9.5) for 10 min, adjusted to pH 2.5 with 20% TFA, and dried under vacuum. Phosphopeptides were subsequently fractionated by hydrophilic interaction liquid chromatography (HILIC) HPLC essentially as described in (*106*). Each resulting fraction was analyzed by liquid chromatography (LC)–MS/MS on an Eksigent NanoLC-Ultra 2D with a cHiPLC-nanoflex system (Eksigent) coupled to an LTQ Orbitrap Velos mass spectrometer (Thermo Fisher Scientific) as described (*108*).

Data were analyzed and quantified using MaxQuant software (*109*) with site FDR set at 0.01. MaxQuant evidence data were loaded into the CoreFlow database and further analyzed with R scripts. Data were normalized between samples (replicates) by aligning the median $\log_2$ ratios of the overall high-confidence data (PEP score <0.01). Reproducibility was estimated on the basis of the variation of the $\log_2$ ratios between samples on each of the high-confidence identified peptides (PEP score <0.01). Both samples separated by HILIC fractionation and by SDS-PAGE showed similar variation. Log_2 ratios between different time points were calculated for each phosphopeptide, and phosphopeptides were considered significantly modulated if their ratios were outside 3 SDs of biological replicates of unphosphorylated peptides either from the same protein (if available) or from all other proteins. NetworKIN predictions were performed as described above.

TRAIL receptor endocytosis assay

This assay was adapted from Akazawa *et al.* (*110*). Briefly, 6×10^5 DLD-1 cells, stably expressing either empty vector or a kinase, were seeded in 12-well tissue-culture plates (BD Falcon) and grown overnight before serum starvation in RPMI medium with 0.1% FBS overnight. The cells were then further starved in serum-free RPMI for 1 hour before being washed in 4°C PBS. FLAG-tagged TRAIL (Enzo Life Sciences), diluted to 400 ng/ml in serum-free RPMI, was preincubated with the M2 antibody recognizing FLAG (2 µg/ml, Sigma, cat#F1804) for 1 hour at 4°C and then added to the PBS-washed cells for 45 min at 4°C. After a further wash in PBS, the cells were incubated with goat anti-mouse antibody conjugated to Alexa 647 (Life Technologies, cat#A-21235) at 4°C for 15 min, and washed again in PBS. The cells were then incubated at 37°C with prewarmed RPMI (no FBS). At the indicated time points, cells were washed with ice-cold PBS and incubated with acid-wash buffer (130 mM NaCl, 2 mM $CaCl_2$, acetic acid to pH 5.0) with shaking for 15 min. After another wash, the cells were detached with trypsin. They were then fixed in BD Cytofix fixation buffer and analyzed with the FACSArray flow cytometer. At least 10,000 events were collected after a forward scatter (FSC) filter of 30K. The single cell population was gated using FSC and side scatter (SSC) parameters. The median value in the "Red" channel of this population was analyzed.

Network modeling

Phenotypic classification of kinases was combined with protein-protein interaction data from the IP-MS and global phosphoproteomics analysis (table S8) in a directed graph network that was analyzed using custom R scripts based on the following R (version 2.15.2) packages: igraph, lattice, latticeExtra, and colorRamps. Directed edges were added for kinase/substrate or SH2 domain–containing protein/substrate pairs. For IP-MS data, "very high stringency for prey frequency" (table S5) interactions were assigned an edge weight of 0.9 and "high stringency for prey frequency" interactions were assigned an edge weight of 0.5. Literature-curated predictions for kinase/substrate pairs were given a score of 0.8, and for all other predictions, the NetworKIN scores were used. To join unconnected kinases (those with no IP-MS data) to the network, additional interactions were obtained from the STRING database (*111*) using an experimental score greater than 0.4 as the cutoff, from GeneMania (*112*), or from literature review. GeneMania interactions were assigned an edge weight of 0.5, literature interactions were given a weight of 0.8, and STRING experimental scores were used for the STRING-curated edges. We constructed three separate networks differentiated by the modulated phosphoproteins at $t = 0$ min, $t = 5$ min, and $t = 60$ min TRAIL stimulation. If a phosphorylation was down-regulated at $t > 0$ min, then the modulated substrate and its predicted partner(s) were connected in the $t = 0$ network and removed for subsequent time points. Conversely, in the case of up-regulation of a phosphosite, the corresponding substrate and partner were assigned to the appropriate later time point.

Paths from a kinase "source" to a kinase or modulated substrate "sink" were obtained using igraph get.shortest.paths function that can provide either the shortest path between two nodes as the minimum number of hops regardless of the edge weights or the best path with the highest sum of weights. Log transformation of probabilities into weights allowed the determination of the routes with maximum product probability on the routes between a "source" and a "sink" node. In the end, we selected an optimal route that was either the best path (highest maximum probability) or the shortest path if the probability of the shortest path was not lower than 25% of the best path probability. The function get.shortest.paths was applied iteratively, by removing each optimal path obtained at the current iteration, to obtain a maximum of 10 disjoint routes. This limit on the total number of optimal routes between a source and a sink node was selected to approximate the median degree number (edges in a node) of 9 and to limit the total duration of the computation.

For each source and sink pair of nodes in the graph, we calculated the combined probability [information flow (I_f)] of the disjoint routes that connect them. The formula used for calculating the combined probability of r independent routes was as follows: $P(\text{any of } r \text{ routes}) = 1 - (1 - P_1)(1 - P_2)...(1 - P_r)$, where P_1, P_2,... P_r are the probabilities on each disjoint route.

On the basis of the above combined probabilities, we constructed a matrix from each of the $t = 0$ min, $t = 5$ min, and $t = 60$ min networks, where the columns correspond to the source, the rows to the sinks, and the

values to the combined probability (I_f). After subtracting the information flow values for $t = 5$ min or $t = 60$ min from $t = 0$ min to obtain ΔI_f values, we applied hierarchical clustering (distance: Euclidean, linkage method: complete) to present the kinases and kinases/modulated substrates that are similar in terms of change in information flow (ΔI_f). Because of the presence of many zero (ΔI_f) values, we focused only on the columns (sources) and rows (sinks) with high information flow (defined as outside of the 93% quantile of the mean $\log_2$ sum of squared ΔI_f for each column and for each row for Fig. 6B and fig. S14A).

SUPPLEMENTARY MATERIALS

www.sciencesignaling.org/cgi/content/full/8/371/rs3/DC1

Fig. S1. Diagram of the method for using the EC-RP sensor to detect CASP3 activity.
Fig. S2. Selected examples of anisotropy measurements for the siRNA screen.
Fig. S3. siRNA screen validation.
Fig. S4. Overexpression screen to identify kinases that affect TRAIL-induced apoptosis.
Fig. S5. Evolutionary tree of the kinome with the apoptosis-modifying kinases indicated.
Fig. S6. Effect of knockdown of apoptosis-modifying kinases in HCT116 and LS174 cells.
Fig. S7. Filtering steps for IP-MS.
Fig. S8. Coimmunoprecipitation of kinase and interacting partners identified as prey in the IP-MS analysis.
Fig. S9. Comparison of interacting partners for kinases identified in previous IP-MS studies.
Fig. S10. Box plot of quantified phosphopeptides for β-catenin (CTNNB1) for the $t = 60$ min/$t = 0$ min ratio.
Fig. S11. Dynamic changes in phosphorylated peptides after TRAIL stimulation.
Fig. S12. Validation of a set of modulated phosphorylated sites by quantitative Western blot.
Fig. S13. Enrichment of apoptosis-modifying kinases by information flow analysis.
Fig. S14. Information flow analysis for $t = 60$ min.
Table S1. Results for genes (including GAPDH) screened in siRNA assay.
Table S2. List of reagents used in this study.
Table S3. Results for kinases screened in cDNA overexpression assay.
Table S4. Union of siRNA and cDNA overexpression assays—combined phenotype.
Table S5. IP-MS filtered results.
Table S6. Preys for kinases from the TRAIL data set that overlap with the CMGC and Interlab reproducibility data sets.
Table S7. List of phosphopeptides identified by global phosphorylation analysis.
Table S8. List of all the protein-protein interactions (edges) used in the information flow analysis.
Table S9. Matrices of information flow (I_f) and change in information flow (ΔI_f) from source to sink.
File S1. Hierarchical clustering of the polarization anisotropy normalized to $t = 0$ min for the siRNA screen.
File S2. Detailed polarization anisotropy measurements for siRNA targets.
File S3. Detailed polarization anisotropy measurements for outliers.
File S4. Flow cytometry measurements in response to TRAIL stimulation for the controls ARAF, CSNK2A1, CASP8, and empty vector.
File S5. Response of each kinase-expressing stable cell line at 2 and 4 hours of TRAIL stimulation.
File S6. Ratios for significantly modulated phosphopeptides after TRAIL stimulation.
File S7. Hierarchical clustering of ΔI_f values at different quantiles.
Reference (*132*)

REFERENCES AND NOTES

1. F. Gonzalvez, A. Ashkenazi, New insights into apoptosis signaling by Apo2L/TRAIL. *Oncogene* **29**, 4752–4765 (2010).
2. D. W. Stuckey, K. Shah, TRAIL on trial: Preclinical advances in cancer therapy. *Trends Mol. Med.* **19**, 685–694 (2013).
3. I. Bozic, T. Antal, H. Ohtsuki, H. Carter, D. Kim, S. Chen, R. Karchin, K. W. Kinzler, B. Vogelstein, M. a. Nowak, Accumulation of driver and passenger mutations during tumor progression. *Proc. Natl. Acad. Sci. U.S.A.* **107**, 18545–18550 (2010).
4. K. M. Boatright, G. S. Salvesen, Mechanisms of caspase activation. *Curr. Opin. Cell Biol.* **15**, 725–731 (2003).
5. J. Lemke, S. von Karstedt, J. Zinngrebe, H. Walczak, Getting TRAIL back on track for cancer therapy. *Cell Death Differ.* **21**, 1350–1364 (2014).
6. M. Russo, A. Mupo, C. Spagnuolo, G. L. Russo, Exploring death receptor pathways as selective targets in cancer therapy. *Biochem. Pharmacol.* **80**, 674–682 (2010).
7. L. Y. Dimberg, C. K. Anderson, R. Camidge, K. Behbakht, A. Thorburn, H. L. Ford, On the TRAIL to successful cancer therapy? Predicting and counteracting resistance against TRAIL-based therapeutics. *Oncogene* **32**, 1341–1350 (2013).
8. E. M. Gibson, E. S. Henson, N. Haney, J. Villanueva, S. B. Gibson, Epidermal growth factor protects epithelial-derived cells from tumor necrosis factor-related apoptosis-inducing ligand-induced apoptosis by inhibiting cytochrome c release. *Cancer Res.* **62**, 488–496 (2002).
9. J. Abdulghani, W. S. El-Deiry, TRAIL receptor signaling and therapeutics. *Expert Opin. Ther. Targets* **14**, 1091–1108 (2010).
10. A. Ashkenazi, Directing cancer cells to self-destruct with pro-apoptotic receptor agonists. *Nat. Rev. Drug Discov.* **7**, 1001–1012 (2008).
11. K. Kandasamy, R. K. Srivastava, Role of the phosphatidylinositol 3′-kinase/PTEN/Akt kinase pathway in tumor necrosis factor-related apoptosis-inducing ligand-induced apoptosis in non-small cell lung cancer cells. *Cancer Res.* **62**, 4929–4937 (2002).
12. C. López-Otín, T. Hunter, The regulatory crosstalk between kinases and proteases in cancer. *Nat. Rev. Cancer* **10**, 278–292 (2010).
13. K. Azijli, B. Weyhenmeyer, G. J. Peters, S. de Jong, F. A. Kruyt, Non-canonical kinase signaling by the death ligand TRAIL in cancer cells: Discord in the death receptor family. *Cell Death Differ.* **20**, 858–868 (2013).
14. S. Fulda, E. Meyer, K. M. Debatin, Inhibition of TRAIL-induced apoptosis by Bcl-2 overexpression. *Oncogene* **21**, 2283–2294 (2002).
15. S. Hinz, A. Trauzold, L. Boenicke, C. Sandberg, S. Beckmann, E. Bayer, H. Walczak, H. Kalthoff, H. Ungefroren, Bcl-XL protects pancreatic adenocarcinoma cells against CD95- and TRAIL-receptor-mediated apoptosis. *Oncogene* **19**, 5477–5486 (2000).
16. S. Van Schaeybroeck, D. M. Kelly, J. Kyula, S. Stokesberry, D. A. Fennell, P. G. Johnston, D. B. Longley, Src and ADAM-17–mediated shedding of transforming growth factor-α is a mechanism of acute resistance to TRAIL. *Cancer Res.* **68**, 8312–8321 (2008).
17. T. Zhou, J. M. Carlson, J. Doyle, Mutation, specialization, and hypersensitivity in highly optimized tolerance. *Proc. Natl. Acad. Sci. U.S.A.* **99**, 2049–2054 (2002).
18. S. Nayak, S. Salim, D. Luan, M. Zai, J. D. Varner, A test of highly optimized tolerance reveals fragile cell-cycle mechanisms are molecular targets in clinical cancer trials. *PLOS One* **3**, e2016 (2008).
19. H. Kitano, A robustness-based approach to systems-oriented drug design. *Nat. Rev. Drug Discov.* **6**, 202–210 (2007).
20. T. Pawson, R. Linding, Network medicine. *FEBS Lett.* **582**, 1266–1270 (2008).
21. I. W. Taylor, R. Linding, D. Warde-Farley, Y. Liu, C. Pesquita, D. Faria, S. Bull, T. Pawson, Q. Morris, J. L. Wrana, Dynamic modularity in protein interaction networks predicts breast cancer outcome. *Nat. Biotechnol.* **27**, 199–204 (2009).
22. D. Breitkreutz, L. Hlatky, E. Rietman, J. A. Tuszynski, Molecular signaling network complexity is correlated with cancer patient survivability. *Proc. Natl. Acad. Sci. U.S.A.* **109**, 9209–9212 (2012).
23. H. Yu, P. M. Kim, E. Sprecher, V. Trifonov, M. Gerstein, The importance of bottlenecks in protein networks: Correlation with gene essentiality and expression dynamics. *PLOS Comput. Biol.* **3**, e59 (2007).
24. S. I. Berger, R. Iyengar, Network analyses in systems pharmacology. *Bioinformatics* **25**, 2466–2472 (2009).
25. P. V. Missiuro, K. Liu, L. Zou, B. C. Ross, G. Zhao, J. S. Liu, H. Ge, Information flow analysis of interactome networks. *PLOS Comput. Biol.* **5**, e1000350 (2009).
26. J. Fasolo, A. Sboner, M. G. Sun, H. Yu, R. Chen, D. Sharon, P. M. Kim, M. Gerstein, M. Snyder, Diverse protein kinase interactions identified by protein microarrays reveal novel connections between cellular processes. *Genes Dev.* **25**, 767–778 (2011).
27. A. Breitkreutz, H. Choi, J. R. Sharom, L. Boucher, V. Neduva, B. Larsen, Z. Y. Lin, B. J. Breitkreutz, C. Stark, G. Liu, J. Ahn, D. Dewar-Darch, T. Reguly, X. Tang, R. Almeida, Z. S. Qin, T. Pawson, A. C. Gingras, A. I. Nesvizhskii, M. Tyers, A global protein kinase and phosphatase interaction network in yeast. *Science* **328**, 1043–1046 (2010).
28. S. Kilpinen, K. Ojala, O. Kallioniemi, Analysis of kinase gene expression patterns across 5681 human tissue samples reveals functional genomic taxonomy of the kinome. *PLOS One* **5**, e15068 (2010).
29. J. G. Albeck, J. M. Burke, B. B. Aldridge, M. Zhang, D. A. Lauffenburger, P. K. Sorger, Quantitative analysis of pathways controlling extrinsic apoptosis in single cells. *Mol. Cell* **30**, 11–25 (2008).
30. M. A. Rizzo, D. W. Piston, High-contrast imaging of fluorescent protein FRET by fluorescence polarization microscopy. *Biophys. J.* **88**, L14–L16 (2005).
31. D. S. Lidke, P. Nagy, B. G. Barisas, R. Heintzmann, J. N. Post, K. A. Lidke, A. H. Clayton, D. J. Arndt-Jovin, T. M. Jovin, Imaging molecular interactions in cells by dynamic and static fluorescence anisotropy (rFLIM and emFRET). *Biochem. Soc. Trans.* **31**, 1020–1027 (2003).
32. Z. W. Li, W. Chu, Y. Hu, M. Delhase, T. Deerinck, M. Ellisman, R. Johnson, M. Karin, The IKKβ subunit of IκB kinase (IKK) is essential for nuclear factor κB activation and prevention of apoptosis. *J. Exp. Med.* **189**, 1839–1845 (1999).
33. G. Khursigara, J. Bertin, H. Yano, H. Moffett, P. S. DiStefano, M. V. Chao, A prosurvival function for the p75 receptor death domain mediated via the caspase recruitment domain receptor-interacting protein 2. *J. Neurosci.* **21**, 5854–5863 (2001).
34. J. V. McCarthy, J. Ni, V. M. Dixit, RIP2 is a novel NF-κB-activating and cell death-inducing kinase. *J. Biol. Chem.* **273**, 16968–16975 (1998).

35. F. C. Kischkel, D. A. Lawrence, A. Chuntharapai, P. Schow, K. J. Kim, A. Ashkenazi, Apo2L/TRAIL-dependent recruitment of endogenous FADD and caspase-8 to death receptors 4 and 5. *Immunity* **12**, 611–620 (2000).
36. J. S. Duncan, J. P. Turowec, K. E. Duncan, G. Vilk, C. Wu, B. Lüscher, S. S.-C. Li, G. B. Gloor, D. W. Litchfield, A peptide-based target screen implicates the protein kinase CK2 in the global regulation of caspase signaling. *Sci. Signal.* **4**, ra30 (2011).
37. M. Varjosalo, S. Keskitalo, A. Van Drogen, H. Nurkkala, A. Vichalkovski, R. Aebersold, M. Gstaiger, The protein interaction landscape of the human CMGC kinase group. *Cell Rep.* **3**, 1306–1320 (2013).
38. G. Guderian, C. Peter, J. Wiesner, A. Sickmann, K. Schulze-Osthoff, U. Fischer, M. Grimmler, RioK1, a new interactor of protein arginine methyltransferase 5 (PRMT5), competes with pICln for binding and modulates PRMT5 complex composition and substrate specificity. *J. Biol. Chem.* **286**, 1976–1986 (2011).
39. D. D. Schlaepfer, M. A. Broome, T. Hunter, Fibronectin-stimulated signaling from a focal adhesion kinase–c-Src complex: Involvement of the Grb2, p130^{cas}, and Nck adaptor proteins. *Mol. Cell. Biol.* **17**, 1702–1713 (1997).
40. K. Vuori, H. Hirai, S. Aizawa, E. Ruoslahti, Introduction of p130^{cas} signaling complex formation upon integrin-mediated cell adhesion: A role for Src family kinases. *Mol. Cell. Biol.* **16**, 2606–2613 (1996).
41. N. Wei, G. Serino, X. W. Deng, The COP9 signalosome: More than a protease. *Trends Biochem. Sci.* **33**, 592–600 (2008).
42. M. Varjosalo, R. Sacco, A. Stukalov, A. van Drogen, M. Planyavsky, S. Hauri, R. Aebersold, K. L. Bennett, J. Colinge, M. Gstaiger, G. Superti-Furga, Interlaboratory reproducibility of large-scale human protein-complex analysis by standardized AP-MS. *Nat. Methods* **10**, 307–314 (2013).
43. H. Takeuchi, T. Takeuchi, J. Gao, L. C. Cantley, M. Hirata, Characterization of PXK as a protein involved in epidermal growth factor receptor trafficking. *Mol. Cell. Biol.* **30**, 1689–1702 (2010).
44. S. D. Conner, S. L. Schmid, Identification of an adaptor-associated kinase, AAK1, as a regulator of clathrin-mediated endocytosis. *J. Cell Biol.* **156**, 921–929 (2002).
45. D. Ricotta, S. D. Conner, S. L. Schmid, K. von Figura, S. Honing, Phosphorylation of the AP2 μ subunit by AAK1 mediates high affinity binding to membrane protein sorting signals. *J. Cell Biol.* **156**, 791–795 (2002).
46. P. V. Hornbeck, J. M. Kornhauser, S. Tkachev, B. Zhang, E. Skrzypek, B. Murray, V. Latham, M. Sullivan, PhosphoSitePlus: A comprehensive resource for investigating the structure and function of experimentally determined post-translational modifications in man and mouse. *Nucleic Acids Res.* **40**, D261–D270 (2012).
47. M. L. Miller, L. J. Jensen, F. Diella, C. Jorgensen, M. Tinti, L. Li, M. Hsiung, S. A. Parker, J. Bordeaux, T. Sicheritz-Ponten, M. Olhovsky, A. Pasculescu, J. Alexander, S. Knapp, N. Blom, P. Bork, S. Li, G. Cesareni, T. Pawson, B. E. Turk, M. B. Yaffe, S. Brunak, R. Linding, Linear motif atlas for phosphorylation-dependent signaling. *Sci. Signal.* **1**, ra2 (2008).
48. R. Linding, L. J. Jensen, G. J. Ostheimer, M. A. van Vugt, C. Jorgensen, I. M. Miron, F. Diella, K. Colwill, L. Taylor, K. Elder, P. Metalnikov, V. Nguyen, A. Pasculescu, J. Jin, J. G. Park, L. D. Samson, J. R. Woodgett, R. B. Russell, P. Bork, M. B. Yaffe, T. Pawson, Systematic discovery of in vivo phosphorylation networks. *Cell* **129**, 1415–1426 (2007).
49. S. E. Ong, B. Blagoev, I. Kratchmarova, D. B. Kristensen, H. Steen, A. Pandey, M. Mann, Stable isotope labeling by amino acids in cell culture, SILAC, as a simple and accurate approach to expression proteomics. *Mol. Cell. Proteomics* **1**, 376–386 (2002).
50. P. V. Hornbeck, I. Chabra, J. M. Kornhauser, E. Skrzypek, B. Zhang, PhosphoSite: A bioinformatics resource dedicated to physiological protein phosphorylation. *Proteomics* **4**, 1551–1561 (2004).
51. R. Linding, L. J. Jensen, A. Pasculescu, M. Olhovsky, K. Colwill, P. Bork, M. B. Yaffe, T. Pawson, NetworKIN: A resource for exploring cellular phosphorylation networks. *Nucleic Acids Res.* **36**, D695-D699 (2008).
52. K. N. Dalby, N. Morrice, F. B. Caudwell, J. Avruch, P. Cohen, Identification of regulatory phosphorylation sites in mitogen-activated protein kinase (MAPK)-activated protein kinase-1a/p90^{rsk} that are inducible by MAPK. *J. Biol. Chem.* **273**, 1496–1505 (1998).
53. K. M. Geraghty, S. Chen, J. E. Harthill, A. F. Ibrahim, R. Toth, N. A. Morrice, F. Vandermoere, G. B. Moorhead, D. G. Hardie, C. MacKintosh, Regulation of multisite phosphorylation and 14-3-3 binding of AS160 in response to IGF-1, EGF, PMA and AICAR. *Biochem. J.* **407**, 231–241 (2007).
54. K. H. Moley, M. M. Mueckler, Glucose transport and apoptosis. *Apoptosis* **5**, 99–105 (2000).
55. X. Wu, X. Tu, K. S. Joeng, M. J. Hilton, D. A. Williams, F. Long, Rac1 activation controls nuclear localization of β-catenin during canonical Wnt signaling. *Cell* **133**, 340–353 (2008).
56. G. Cantarella, G. Di Benedetto, S. Pezzino, N. Risuglia, R. Bernardini, TRAIL-related neurotoxicity implies interaction with the Wnt pathway in human neuronal cells in vitro. *J. Neurochem.* **105**, 1915–1923 (2008).
57. I. Szivak, N. Lamb, L. M. Heilmeyer, Subcellular localization and structural function of endogenous phosphorylated phosphatidylinositol 4-kinase (PI4K92). *J. Biol. Chem.* **281**, 16740–16749 (2006).
58. D. V. Bulavin, Y. Higashimoto, I. J. Popoff, W. A. Gaarde, V. Basrur, O. Potapova, E. Appella, A. J. Fornace Jr., Initiation of a G2/M checkpoint after ultraviolet radiation requires p38 kinase. *Nature* **411**, 102–107 (2001).
59. B. Aressy, B. Ducommun, Cell cycle control by the CDC25 phosphatases. *Anticancer Agents Med. Chem.* **8**, 818–824 (2008).
60. Y. Inoue, M. Kitagawa, Y. Taya, Phosphorylation of pRB at Ser612 by Chk1/2 leads to a complex between pRB and E2F-1 after DNA damage. *EMBO J.* **26**, 2083–2093 (2007).
61. K. Vancompernolle, T. Boonefaes, M. Mann, W. Fiers, J. Grooten, Tumor necrosis factor-induced microtubule stabilization mediated by hyperphosphorylated oncoprotein 18 promotes cell death. *J. Biol. Chem.* **275**, 33876–33882 (2000).
62. K. G. Drosopoulos, M. L. Roberts, L. Cermak, T. Sasazuki, S. Shirasawa, L. Andera, A. Pintzas, Transformation by oncogenic *RAS* sensitizes human colon cells to TRAIL-induced apoptosis by up-regulating death receptor 4 and death receptor 5 through a MEK-dependent pathway. *J. Biol. Chem.* **280**, 22856–22867 (2005).
63. D. Ovcharenko, K. Kelnar, C. Johnson, N. Leng, D. Brown, Genome-scale microRNA and small interfering RNA screens identify small RNA modulators of TRAIL-induced apoptosis pathway. *Cancer Res.* **67**, 10782–10788 (2007).
64. P. Aza-Blanc, C. L. Cooper, K. Wagner, S. Batalov, Q. L. Deveraux, M. P. Cooke, Identification of modulators of TRAIL-induced apoptosis via RNAi-based phenotypic screening. *Mol. Cell* **12**, 627–637 (2003).
65. D. Kranz, M. Boutros, A synthetic lethal screen identifies FAT1 as an antagonist of caspase-8 in extrinsic apoptosis. *EMBO J.* **33**, 181–197 (2014).
66. B. R. Chakravarthy, T. Walker, I. Rasquinha, I. E. Hill, J. P. MacManus, Activation of DNA-dependent protein kinase may play a role in apoptosis of human neuroblastoma cells. *J. Neurochem.* **72**, 933–942 (1999).
67. A. Bharti, S. K. Kraeft, M. Gounder, P. Pandey, S. Jin, Z. M. Yuan, S. P. Lees-Miller, R. Weichselbaum, D. Weaver, L. B. Chen, D. Kufe, S. Kharbanda, Inactivation of DNA-dependent protein kinase by protein kinase Cδ: Implications for apoptosis. *Mol. Cell. Biol.* **18**, 6719–6728 (1998).
68. S. Wang, M. Guo, H. Ouyang, X. Li, C. Cordon-Cardo, A. Kurimasa, D. J. Chen, Z. Fuks, C. C. Ling, G. C. Li, The catalytic subunit of DNA-dependent protein kinase selectively regulates p53-dependent apoptosis but not cell-cycle arrest. *Proc. Natl. Acad. Sci. U.S.A.* **97**, 1584–1588 (2000).
69. G. R. Panta, S. Kaur, L. G. Cavin, M. L. Cortes, F. Mercurio, L. Lothstein, T. W. Sweatman, M. Israel, M. Arsura, ATM and the catalytic subunit of DNA-dependent protein kinase activate NF-κB through a common MEK/extracellular signal-regulated kinase/p90^{rsk} signaling pathway in response to distinct forms of DNA damage. *Mol. Cell. Biol.* **24**, 1823–1835 (2004).
70. S. E. Tran, T. H. Holmstrom, M. Ahonen, V. M. Kahari, J. E. Eriksson, MAPK/ERK overrides the apoptotic signaling from Fas, TNF, and TRAIL receptors. *J. Biol. Chem.* **276**, 16484–16490 (2001).
71. A. D. Durbin, G. R. Somers, M. Forrester, M. Pienkowska, G. E. Hannigan, D. Malkin, JNK1 determines the oncogenic or tumor-suppressive activity of the integrin-linked kinase in human rhabdomyosarcoma. *J. Clin. Invest.* **119**, 1558–1570 (2009).
72. F. Hess, D. Estrugo, A. Fischer, C. Belka, N. Cordes, Integrin-linked kinase interacts with caspase-9 and -8 in an adhesion-dependent manner for promoting radiation-induced apoptosis in human leukemia cells. *Oncogene* **26**, 1372–1384 (2007).
73. K. A. Janes, J. G. Albeck, S. Gaudet, P. K. Sorger, D. A. Lauffenburger, M. B. Yaffe, A systems model of signaling identifies a molecular basis set for cytokine-induced apoptosis. *Science* **310**, 1646–1653 (2005).
74. N. Suzuki, T. Saito, IRAK-4—A shared NF-κB activator in innate and acquired immunity. *Trends Immunol.* **27**, 566–572 (2006).
75. S.-C. Lin, Y.-C. Lo, H. Wu, Helical assembly in the MyD88–IRAK4–IRAK2 complex in TLR/IL-1R signalling. *Nature* **465**, 885–890 (2010).
76. S. K. Radhakrishnan, S. Kamalakaran, Pro-apoptotic role of NF-κB: Implications for cancer therapy. *Biochim. Biophys. Acta* **1766**, 53–62 (2006).
77. S. Senthivinayagam, P. Mishra, S. K. Paramasivam, S. Yallapragada, M. Chatterjee, L. Wong, A. Rana, B. Rana, Caspase-mediated cleavage of β-catenin precedes drug-induced apoptosis in resistant cancer cells. *J. Biol. Chem.* **284**, 13577–13588 (2009).
78. C. D. Austin, D. A. Lawrence, A. A. Peden, E. E. Varfolomeev, K. Totpal, A. M. De Mazière, J. Klumperman, D. Arnott, V. Pham, R. H. Scheller, A. Ashkenazi, Death-receptor activation halts clathrin-dependent endocytosis. *Proc. Natl. Acad. Sci. U.S.A.* **103**, 10283–10288 (2006).
79. S. L. Kohlhaas, A. Craxton, X. M. Sun, M. J. Pinkoski, G. M. Cohen, Receptor-mediated endocytosis is not required for tumor necrosis factor-related apoptosis-inducing ligand (TRAIL)-induced apoptosis. *J. Biol. Chem.* **282**, 12831–12841 (2007).
80. J. J. Song, M. J. Szczepanski, S. Y. Kim, J. H. Kim, J. Y. An, Y. T. Kwon, M. A. Alcala Jr., D. L. Bartlett, Y. J. Lee, c-Cbl-mediated degradation of TRAIL receptors is responsible for

the development of the early phase of TRAIL resistance. *Cell. Signal.* 22, 553–563 (2010).
81. J. V. Abella, M. Park, Breakdown of endocytosis in the oncogenic activation of receptor tyrosine kinases. *Am. J. Physiol. Endocrinol. Metab.* **296**, E973–E984 (2009).
82. Z. Jin, E. R. McDonald 3rd, D. T. Dicker, W. S. El-Deiry, Deficient tumor necrosis factor-related apoptosis-inducing ligand (TRAIL) death receptor transport to the cell surface in human colon cancer cells selected for resistance to TRAIL-induced apoptosis. *J. Biol. Chem.* **279**, 35829–35839 (2004).
83. X. Wu, R. Jiang, M. Q. Zhang, S. Li, Network-based global inference of human disease genes. *Mol. Syst. Biol.* **4**, 189 (2008).
84. M. Oti, B. Snel, M. A. Huynen, H. G. Brunner, Predicting disease genes using protein–protein interactions. *J. Med. Genet.* **43**, 691–698 (2006).
85. O. Vanunu, O. Magger, E. Ruppin, T. Shlomi, R. Sharan, Associating genes and protein complexes with disease via network propagation. *PLOS Comput. Biol.* **6**, e1000641 (2010).
86. M. Nakanishi, H. Ando, N. Watanabe, K. Kitamura, K. Ito, H. Okayama, T. Miyamoto, T. Agui, M. Sasaki, Identification and characterization of human Wee1B, a new member of the Wee1 family of Cdk-inhibitory kinases. *Genes Cells* **5**, 839–847 (2000).
87. S. Gottipati, N. L. Rao, W. P. Fung-Leung, IRAK1: A critical signaling mediator of innate immunity. *Cell. Signal.* **20**, 269–276 (2008).
88. S. Etienne-Manneville, A. Hall, Cell polarity: Par6, aPKC and cytoskeletal crosstalk. *Curr. Opin. Cell Biol.* **15**, 67–72 (2003).
89. M. Leitges, L. Sanz, P. Martin, A. Duran, U. Braun, J. F. Garcia, F. Camacho, M. T. Diaz-Meco, P. D. Rennert, J. Moscat, Targeted disruption of the ζPKC gene results in the impairment of the NF-κB pathway. *Mol. Cell* **8**, 771–780 (2001).
90. S. Bialik, A. Kimchi, The death-associated protein kinases: Structure, function, and beyond. *Annu. Rev. Biochem.* **75**, 189–210 (2006).
91. Y. Huang, L. Chen, L. Guo, T. R. Hupp, Y. Lin, Evaluating DAPK as a therapeutic target. *Apoptosis* **19**, 371–386 (2014).
92. M. Sarker, C. Ruiz-Ruiz, A. Lopez-Rivas, Activation of protein kinase C inhibits TRAIL-induced caspases activation, mitochondrial events and apoptosis in a human leukemic T cell line. *Cell Death Differ.* **8**, 172–181 (2001).
93. P. Sridevi, M. K. Nhiayi, R. L. Setten, J. Y. Wang, Persistent inhibition of ABL tyrosine kinase causes enhanced apoptotic response to TRAIL and disrupts the pro-apoptotic effect of chloroquine. *PLOS One* **8**, e77495 (2013).
94. J. F. Rual, T. Hirozane-Kishikawa, T. Hao, N. Bertin, S. Li, A. Dricot, N. Li, J. Rosenberg, P. Lamesch, P. O. Vidalain, T. R. Clingingsmith, J. L. Hartley, D. Esposito, D. Cheo, T. Moore, B. Simmons, R. Sequerra, S. Bosak, L. Doucette-Stamm, C. Le Peuch, J. Vandenhaute, M. E. Cusick, J. S. Albala, D. E. Hill, M. Vidal, Human ORFeome version 1.1: A platform for reverse proteomics. *Genome Res.* **14**, 2128–2135 (2004).
95. R. Kikuno, T. Nagase, M. Waki, O. Ohara, HUGE: A database for human large proteins identified in the Kazusa cDNA sequencing project. *Nucleic Acids Res.* **30**, 166–168 (2002).
96. J. Park, Y. Hu, T. V. Murthy, F. Vannberg, B. Shen, A. Rolfs, J. E. Hutti, L. C. Cantley, J. Labaer, E. Harlow, L. Brizuela, Building a human kinase gene repository: Bioinformatics, molecular cloning, and functional validation. *Proc. Natl. Acad. Sci. U.S.A.* **102**, 8114–8119 (2005).
97. M. Varjosalo, M. Bjorklund, F. Cheng, H. Syvanen, T. Kivioja, S. Kilpinen, Z. Sun, O. Kallioniemi, H. G. Stunnenberg, W. W. He, P. Ojala, J. Taipale, Application of active and kinase-deficient kinome collection for identification of kinases regulating hedgehog signaling. *Cell* **133**, 537–548 (2008).
98. M. Olhovsky, K. Williton, A. Y. Dai, A. Pasculescu, J. P. Lee, M. Goudreault, C. D. Wells, J. G. Park, A. C. Gingras, R. Linding, T. Pawson, K. Colwill, OpenFreezer: A reagent information management software system. *Nat. Methods* **8**, 612–613 (2011).
99. F. Girdler, K. E. Gascoigne, P. A. Eyers, S. Hartmuth, C. Crafter, K. M. Foote, N. J. Keen, S. S. Taylor, Validating Aurora B as an anti-cancer drug target. *J. Cell Sci.* **119**, 3664–3675 (2006).
100. A. Pasculescu, E. M. Schoof, P. Creixell, Y. Zheng, M. Olhovsky, R. Tian, J. So, R. D. Vanderlaan, T. Pawson, R. Linding, K. Colwill, CoreFlow: A computational platform for integration, analysis and modeling of complex biological data. *J. Proteomics* **100**, 167–173 (2014).
101. R. M. Pitti, S. A. Marsters, S. Ruppert, C. J. Donahue, A. Moore, A. Ashkenazi, Induction of apoptosis by Apo-2 ligand, a new member of the tumor necrosis factor cytokine family. *J. Biol. Chem.* **271**, 12687–12690 (1996).
102. N. Bisson, D. A. James, G. Ivosev, S. A. Tate, R. Bonner, L. Taylor, T. Pawson, Selected reaction monitoring mass spectrometry reveals the dynamics of signaling through the GRB2 adaptor. *Nat. Biotechnol.* **29**, 653–658 (2011).
103. G. Liu, J. Zhang, B. Larsen, C. Stark, A. Breitkreutz, Z. Y. Lin, B. J. Breitkreutz, Y. Ding, K. Colwill, A. Pasculescu, T. Pawson, J. L. Wrana, A. I. Nesvizhskii, B. Raught, M. Tyers, A. C. Gingras, ProHits: Integrated software for mass spectrometry-based interaction proteomics. *Nat. Biotechnol.* **28**, 1015–1017 (2010).
104. S. A. Beausoleil, J. Villen, S. A. Gerber, J. Rush, S. P. Gygi, A probability-based approach for high-throughput protein phosphorylation analysis and site localization. *Nat. Biotechnol.* **24**, 1285–1292 (2006).
105. C. Jorgensen, A. Sherman, G. I. Chen, A. Pasculescu, A. Poliakov, M. Hsiung, B. Larsen, D. G. Wilkinson, R. Linding, T. Pawson, Cell-specific information processing in segregating populations of Eph receptor ephrin–expressing cells. *Science* **326**, 1502–1509 (2009).
106. C. P. Albuquerque, M. B. Smolka, S. H. Payne, V. Bafna, J. Eng, H. Zhou, A multidimensional chromatography technology for in-depth phosphoproteome analysis. *Mol. Cell. Proteomics* **7**, 1389–1396 (2008).
107. T. E. Thingholm, O. N. Jensen, P. J. Robinson, M. R. Larsen, SIMAC (sequential elution from IMAC), a phosphoproteomics strategy for the rapid separation of monophosphorylated from multiply phosphorylated peptides. *Mol. Cell. Proteomics* **7**, 661–671 (2008).
108. M. R. Girotti, M. Pedersen, B. Sanchez-Laorden, A. Viros, S. Turajlic, D. Niculescu-Duvaz, A. Zambon, J. Sinclair, A. Hayes, M. Gore, P. Lorigan, C. Springer, J. Larkin, C. Jorgensen, R. Marais, Inhibiting EGF receptor or SRC family kinase signaling overcomes BRAF inhibitor resistance in melanoma. *Cancer Discov* **3**, 158–167 (2013).
109. J. Cox, M. Mann, MaxQuant enables high peptide identification rates, individualized p.p.b.-range mass accuracies and proteome-wide protein quantification. *Nat. Biotechnol.* **26**, 1367–1372 (2008).
110. Y. Akazawa, J. L. Mott, S. F. Bronk, N. W. Werneburg, A. Kahraman, M. E. Guicciardi, X. W. Meng, S. Kohno, V. H. Shah, S. H. Kaufmann, M. A. McNiven, G. J. Gores, Death receptor 5 internalization is required for lysosomal permeabilization by TRAIL in malignant liver cell lines. *Gastroenterology* **136**, 2365–2376.e7 (2009).
111. D. Szklarczyk, A. Franceschini, M. Kuhn, M. Simonovic, A. Roth, P. Minguez, T. Doerks, M. Stark, J. Muller, P. Bork, L. J. Jensen, C. von Mering, The STRING database in 2011: Functional interaction networks of proteins, globally integrated and scored. *Nucleic Acids Res.* **39**, D561–D568 (2011).
112. D. Warde-Farley, S. L. Donaldson, O. Comes, K. Zuberi, R. Badrawi, P. Chao, M. Franz, C. Grouios, F. Kazi, C. T. Lopes, A. Maitland, S. Mostafavi, J. Montojo, Q. Shao, G. Wright, G. D. Bader, Q. Morris, The GeneMANIA prediction server: Biological network integration for gene prioritization and predicting gene function. *Nucleic Acids Res.* **38**, W214–W220 (2010).
113. C. J. Gloeckner, K. Boldt, A. Schumacher, R. Roepman, M. Ueffing, A novel tandem affinity purification strategy for the efficient isolation and characterisation of native protein complexes. *Proteomics* **7**, 4228–4234 (2007).
114. S. Choi, W. Hao, C. K. Chen, M. I. Simon, Gene expression profiles of light-induced apoptosis in arrestin/rhodopsin kinase-deficient mouse retinas. *Proc. Natl. Acad. Sci. U.S.A.* **98**, 13096–13101 (2001).
115. W. Hao, A. Wenzel, M. S. Obin, C. K. Chen, E. Brill, N. V. Krasnoperova, P. Eversole-Cire, Y. Kleyner, A. Taylor, M. I. Simon, C. Grimm, C. E. Reme, J. Lem, Evidence for two apoptotic pathways in light-induced retinal degeneration. *Nat. Genet.* **32**, 254–260 (2002).
116. C. K. Chen, M. E. Burns, M. Spencer, G. A. Niemi, J. Chen, J. B. Hurley, D. A. Baylor, M. I. Simon, Abnormal photoresponses and light-induced apoptosis in rods lacking rhodopsin kinase. *Proc. Natl. Acad. Sci. U.S.A.* **96**, 3718–3722 (1999).
117. G. Tang, J. Yang, Y. Minemoto, A. Lin, Blocking caspase-3-mediated proteolysis of IKKβ suppresses TNF-α-induced apoptosis. *Mol. Cell* **8**, 1005–1016 (2001).
118. Q. Li, D. Van Antwerp, F. Mercurio, K. F. Lee, I. M. Verma, Severe liver degeneration in mice lacking the IκB kinase 2 gene. *Science* **284**, 321–325 (1999).
119. A. A. Troussard, N. M. Mawji, C. Ong, A. Mui, R. St -Arnaud, S. Dedhar, Conditional knock-out of integrin-linked kinase demonstrates an essential role in protein kinase B/Akt activation. *J. Biol. Chem.* **278**, 22374–22378 (2003).
120. S. Persad, S. Attwell, V. Gray, M. Delcommenne, A. Troussard, J. Sanghera, S. Dedhar, Inhibition of integrin-linked kinase (ILK) suppresses activation of protein kinase B/Akt and induces cell cycle arrest and apoptosis of PTEN-mutant prostate cancer cells. *Proc. Natl. Acad. Sci. U.S.A.* **97**, 3207–3212 (2000).
121. S. Attwell, C. Roskelley, S. Dedhar, The integrin-linked kinase (ILK) suppresses anoikis. *Oncogene* **19**, 3811–3815 (2000).
122. J. Pan, J. Zhang, A. Hill, P. Lapan, S. Berasi, B. Bates, C. Miller, S. Haney, A kinome-wide siRNA screen identifies multiple roles for protein kinases in hypoxic stress adaptation, including roles for IRAK4 and GAK in protection against apoptosis in VHL$^{-/-}$ renal carcinoma cells, despite activation of the NF-κB pathway. *J. Biomol. Screen.* **18**, 782–796 (2013).
123. L. Novikova, N. Czymmeck, A. Deuretzbacher, F. Buck, K. Richter, A. N. Weber, M. Aepfelbacher, K. Ruckdeschel, Cell death triggered by *Yersinia enterocolitica* identifies processing of the proinflammatory signal adapter MyD88 as a general event in the execution of apoptosis. *J. Immunol.* **192**, 1209–1219 (2014).
124. R. Srivastava, D. Geng, Y. Liu, L. Zheng, Z. Li, M. A. Joseph, C. McKenna, N. Bansal, A. Ochoa, E. Davila, Augmentation of therapeutic responses in melanoma by inhibition of IRAK-1,-4. *Cancer Res.* **72**, 6209–6216 (2012).
125. M. L. Lin, J. H. Park, T. Nishidate, Y. Nakamura, T. Katagiri, Involvement of maternal embryonic leucine zipper kinase (MELK) in mammary carcinogenesis through interaction with Bcl-G, a pro-apoptotic member of the Bcl-2 family. *Breast Cancer Res.* **9**, R17 (2007).

126. N. Inohara, L. del Peso, T. Koseki, S. Chen, G. Nunez, RICK, a novel protein kinase containing a caspase recruitment domain, interacts with CLARP and regulates CD95-mediated apoptosis. *J. Biol. Chem.* **273**, 12296–12300 (1998).
127. D. Piazzolla, K. Meissl, L. Kucerova, C. Rubiolo, M. Baccarini, Raf-1 sets the threshold of Fas sensitivity by modulating Rok-α signaling. *J. Cell Biol.* **171**, 1013–1022 (2005).
128. J. Shi, L. Wei, Rho kinase in the regulation of cell death and survival. *Arch. Immunol. Ther. Exp.* **55**, 61–75 (2007).
129. Y. Song, B. Q. Hoang, D. D. Chang, ROCK-II-induced membrane blebbing and chromatin condensation require actin cytoskeleton. *Exp. Cell Res.* **278**, 45–52 (2002).
130. N. Azoitei, A. Brey, T. Busch, S. Fulda, G. Adler, T. Seufferlein, Thirty-eight-negative kinase 1 (TNK1) facilitates TNFα-induced apoptosis by blocking NF-κB activation. *Oncogene* **26**, 6536–6545 (2007).
131. M. C. Henderson, I. M. Gonzales, S. Arora, A. Choudhary, J. M. Trent, D. D. Von Hoff, S. Mousses, D. O. Azorsa, High-throughput RNAi screening identifies a role for TNK1 in growth and survival of pancreatic cancer cells. *Mol. Cancer Res.* **9**, 724–732 (2011).
132. I. Letunic, P. Bork, Interactive Tree Of Life (iTOL): An online tool for phylogenetic tree display and annotation. *Bioinformatics* **23**, 127–128 (2007).

Acknowledgments: We would like to thank the members of the Pawson laboratory for their experimental support and helpful discussions. Thanks to R. Bristow for experimental support. We would also like to thank A. Datti and T. Sun from the Robotics Core Facility for technical assistance, M. Parsons from the Flow Cytometry Facility, and the Centre for Applied Genomics for sequencing assistance. Thanks to A. Ashkenazi and E. Petsalakis for comments on the manuscript. Thanks also to A. Ashkenazi for the gift of recombinant Apo2L/TRAIL, to S. Taylor for the DLD-1 LacZeo/TO cells, and to S. Gaudet for the EC-RP sensor. This paper is dedicated to the memory of Tony Pawson. **Funding:** J. So was supported by a fellowship from the Canadian Institutes of Health Research. T.P. was supported by grants from the Ontario Research Fund GL2 program, Genome Canada through the Ontario Genomics Institute, and CIHR (MOP-6849). C.J. is supported by a CR-UK Career Establishment Award (C37293/A12905). R.L. was funded by The Lundbeck Foundation and the European Research Council under the European Union's Seventh Framework Programme (FP/2007-2013)/ERC Grant (KINOMEDRIFT) and was supported by the VKR-funded Instrument Center for Systems Proteomics (VKR022758). **Author contributions:** K.C., C.J., and R.L. conceived, initiated, and led the strategic development of the project. R.L., T.P., C.J., and K.C. oversaw the project. A.Y.D., K.W., J.G., M.B.-R., A.K., and R.W. carried out the cloning of the human kinases. J.W.D. and J.L.W. supported the cloning of kinases. K.W. and A.Y.D. performed the immunoprecipitation of kinases. J. So performed the phenotyping screens, endocytosis assays, and phosphoproteomics validation assays. C.J., J. So, and J. Si. performed the SILAC MS experiment. V.N. and A.J. performed MS. K.W. performed the co-IP validation. P.C., E.M.S., and R.L. provided kinase predictions. P.C., A.P., J. So, and R.L. performed the data analysis and modeling. K.C. and M.O. provided database and cell line management support. J. So, K.C., and C.J. wrote the paper. **Competing interests:** The authors declare that they have no competing interests. **Data and materials availability:** The caspase-3 activity sensor (EC-RP) was a gift from S. Gaudet obtained through a material transfer agreement (MTA). The DLD-1 LacZeo/TO cell line was provided by S. Taylor through an MTA. The Apo2L/TRAIL reagent was obtained from Avi Ashkenazi (Genentech) through an MTA. Reagents are available upon request to colwill@lunenfeld.ca. All raw MS data are available through the MassIVE Web portal (http://massive.ucsd.edu, MassIVE ID: MSV000078989), and the results can be viewed at http://pawsonlab.mshri.on.ca/KinaseTrail/. The protein interactions from this publication have been submitted to the IMEx (www.imexconsortium.org) consortium through IntAct and assigned the identifier IM-23674. A resource of our study is presented at http://pawsonlab.mshri.on.ca/KinaseTrail/.

Submitted 17 July 2014
Accepted 20 March 2015
Final Publication 7 April 2015
10.1126/scisignal.2005700
Citation: J. So, A. Pasculescu, A. Y. Dai, K. Williton, A. James, V. Nguyen, P. Creixell, E. M. Schoof, J. Sinclair, M. Barrios-Rodiles, J. Gu, A. Krizus, R. Williams, M. Olhovsky, J. W. Dennis, J. L. Wrana, R. Linding, C. Jorgensen, T. Pawson, K. Colwill, Integrative analysis of kinase networks in TRAIL-induced apoptosis provides a source of potential targets for combination therapy. *Sci. Signal.* **8**, rs3 (2015).

Integrative analysis of kinase networks in TRAIL-induced apoptosis provides a source of potential targets for combination therapy

Jonathan So, Adrian Pasculescu, Anna Y. Dai, Kelly Williton, Andrew James, Vivian Nguyen, Pau Creixell, Erwin M. Schoof, John Sinclair, Miriam Barrios-Rodiles, Jun Gu, Aldis Krizus, Ryan Williams, Marina Olhovsky, James W. Dennis, Jeffrey L. Wrana, Rune Linding, Claus Jorgensen, Tony Pawson and Karen Colwill
(April 7, 2015)
Science Signaling **8** (371), rs3. [doi: 10.1126/scisignal.2005700]

Science Signaling (ISSN 1937-9145) is published weekly, except the last December, by the American Association for the Advancement of Science, 1200 New York Avenue, NW, Washington, DC 20005.